ISSN 2732–0189 (Online)
ISSN 1586–2070 (Print)

JOURNAL OF COMPUTATIONAL AND APPLIED MECHANICS

An Open Access International Journal

Published by the University of Miskolc

VOLUME 20, NUMBER 2 (2025)

MISKOLC UNIVERSITY PRESS

ISSN 2732–0189 (Online)
ISSN 1586–2070 (Print)

JOURNAL OF COMPUTATIONAL AND APPLIED MECHANICS

An Open Access International Journal

Published by the University of Miskolc

VOLUME 20 NUMBER 2 (2025)

MISKOLC UNIVERSITY PRESS

Journal of Computational and Applied Mechanics, Vol. 20, No. 2, (2025), pp. 71–92
DOI: 10.32973/jcam.2025.003

INITIAL STATE DEPENDENCE OF THERMO-MECHANICAL COUPLING IN HEAT CONDUCTION NEAR THE LIQUID-VAPOR CRITICAL POINT

Kristóf Tóth
Department of Energy Engineering, Faculty of Mechanical Engineering,
Budapest University of Technology and Economics
Műegyetem rkp. 3., H-1111 Budapest, Hungary
kristofferenctoth@edu.bme.hu

Mátyás Szücs
Department of Energy Engineering, Faculty of Mechanical Engineering,
Budapest University of Technology and Economics
Műegyetem rkp. 3., H-1111 Budapest, Hungary;
Institute for Particle and Nuclear Physics, HUN-REN Wigner Research Centre for Physics
Konkoly-Thege Miklós út 29–33, H-1121 Budapest, Hungary;
Montavid Thermodynamic Research Group,
Society for the Unity of Science and Technology
Lovas út 18., H-1012 Budapest, Hungary
szucs.matyas@gpk.bme.hu

[Received: December 13, 2025; Accepted: February 23, 2026]

Abstract. In the vicinity of the liquid–vapor critical point, fluids behave in a strongly compressible manner and their thermophysical parameters exhibit significant state-dependence, leading to an intense coupling of the mechanical and the thermal processes. For instance, the piston effect is a coupled thermo-acoustic phenomenon when close to a heated surface a thermal boundary layer forms in the fluid, which expands due to the relatively large value of the isobaric thermal expansion coefficient. Accordingly, the expansion of the boundary layer caused by its temperature change excites pressure waves in the fluid, which also transports thermal energy during its propagation. Therefore, the propagation of the temperature at the speed of sound can be observed, in contrast to the delayed nature of the diffusive heat propagation. In this study, an effective heat conduction model is investigated in the linear approximation, which neglects acoustic propagation, but considers the effect of thermal expansion. We identify and analyze the state-dependent parameters influencing the dynamics and explore through numerical simulations how the initial conditions affect the process .

Mathematical Subject Classification: 76N06, 80M20
Keywords: supercritical fluids, heat conduction, thermal expansion, coupled problems, piston effect, finite difference method

1. Introduction

Liquids and gases can only be distinguished within a limited region of the thermodynamic state space. The coexistence curve terminates at the liquid-vapor critical point, where the thermophysical properties of the two phases become increasingly

similar. In the critical point, phase boundaries vanish; thus, the heat of vaporization approaches zero. The critical point is a material-specific property defined by its temperature, pressure, and density. Above a critical temperature and pressure, the fluid exhibits both liquid and gas characteristics, allowing continuous transformation between these states without a phase transition [1].

In the vicinity of the critical point, the fluid becomes strongly compressible and in parallel, its thermophysical properties exhibit rapid changes, even by orders of magnitude [2, 3]. Although the design of systems operating with supercritical fluids is complicated by anomalies in the material properties and corrosion risks, the advantages of supercritical fluids are widely exploited in industrial and energy applications. For instance, in the food and pharmaceutical industries, supercritical carbon dioxide extraction is used for decaffeination, aroma recovery, and sterilization processes, taking advantage of the fluid's excellent solvability and diffusion characteristics [4]. In the energy sector, supercritical steam cycles and fourth-generation nuclear reactors employing supercritical coolants enable significant efficiency improvements, while supercritical carbon dioxide based power systems offer compact turbine and heat exchanger solutions [5, 6]. Furthermore, the usage of supercritical carbon dioxide offers new perspectives for enhanced geothermal systems to extract heat from hot dry rocks [7, 8]. This technology may also be integrated in carbon sequestration strategies. Since differences between liquid and gas vanish in supercritical states, phenomena such as boiling crisis can be avoided; however, other technical difficulties may occur, such as heat transfer deterioration [9]. Therefore, the proper design and safe operation of supercritical systems require a thorough understanding of the coupled thermomechanical phenomena that emerge in supercritical fluids.

Near the critical point, the compressibility and the state dependence of the material parameters result in the coupling of thermal and flow processes [10, 11]. Consider a tank filled with a fluid near its critical point. When the wall of the tank is heated, a thermal boundary layer forms near the heated surface and expands due to the relatively large thermal expansion coefficient, while the expanding boundary layer compresses the bulk fluid like a piston. This phenomenon, known as the *piston effect*, results in an almost isentropic pressure rise, which leads to a rapid temperature increase in the bulk, contrasting with the slow nature of the diffusive heat transfer. Consequently, heat conduction is significantly influenced by thermal expansion.

Although previous works (*e.g.,* [12–14]) thoroughly analyze thermo-mechanical coupling and the piston effect, these studies generally consider a fixed initial thermodynamic state; hence, the sensitivity of the phenomenon to slight variations in the initial temperature or pressure has not been explicitly analyzed. While the experimental investigations carried out during the SpaceLab D2 mission [15] explored the piston effect at several initial temperatures, the focus was the empirical confirmation of fast temperature propagation rather than a systematic characterization of the initial-state dependence. In this work, we investigate the dependence of the piston effect on the initial thermodynamic state. Although our analysis relies on linearized equations, the intense variations in the material properties near the critical point lead to unexpected behavior. We identify the parameters governing the dynamics, thereby explaining why

processes initiated under nearly identical conditions may exhibit significantly different transients. These findings are also corroborated through numerical simulations. In summary, the present study clarifies and quantifies the role of the initial state in the dynamics of the piston effect.

Our long-term goal is to investigate the effect of material nonlinearities on heat conduction near the critical point. This work also serves as a preliminary study for this future investigation and as a preparation for the numerical methodology required for the analysis of nonlinear behavior.

The first results have been presented at the Student's Scientific Conference at Budapest University of Technology and Economics by Kristóf Tóth with the supervision of Mátyás Szücs [16]. Here we present a more systematic background for the phenomenon and an extended analysis of the material behavior near the critical point.

2. The piston effect

Anomalies of material properties near the critical point lead to peculiar heat transfer phenomena. Usually, heat conduction in a medium which is at rest with respect to an inertial reference system is described via the heat equation

$$\varrho c_p \frac{\partial T}{\partial t} = \nabla \cdot (\lambda \nabla T)\,, \tag{2.1}$$

where T is the temperature field (*i.e.,* a time and space dependent function), ϱ, c_p and λ are the density, the isobaric specific heat capacity and the thermal conductivity, respectively, $\frac{\partial}{\partial t}$ is the partial time derivative and ∇ is the nabla operator, which – depending on the vectorial multiplication – denotes the gradient or divergence. Assuming constant thermophysical parameters, (2.1) can be reformulated to

$$\frac{\partial T}{\partial t} = \alpha \nabla^2 T \tag{2.2}$$

with the thermal diffusivity $\alpha = \frac{\lambda}{\varrho c_p}$ and the Laplace operator ∇^2. By introducing a characteristic length scale ℓ, the *thermal diffusion time scale* can be defined as

$$t_\mathrm{d} = \frac{\ell^2}{\alpha}, \tag{2.3}$$

which characterizes diffusive propagation. At the critical point, the isobaric specific heat capacity diverges, thus thermal diffusivity tends to zero. Figure 1 presents the state dependence of the thermal diffusivity of carbon dioxide, calculated from the Span–Wagner equation of state [17] together with the reference thermal-conductivity correlation [18]. Consequently, near the critical point, heat conduction is expected to decelerate drastically, which is referred to in the literature as 'critical slowing down' [10, 11].

In contrast, experiments conducted under terrestrial conditions have shown rapid temperature homogenization in supercritical fluids, which contradicts the previous theoretical prediction. This observation was explained by convective mixing caused by buoyancy, but in a space experiment, the same rapid temperature homogenization

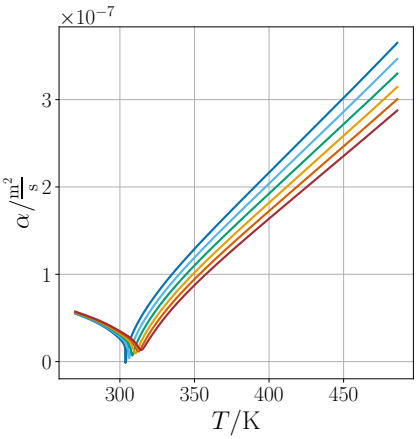

Figure 1. Temperature dependence of the thermal diffusivity of carbon dioxide along the isobaric lines $\approx 1p_c$, $1.05p_c$, $1.1p_c$, $1.15p_c$, $1.2p_c$ and $1.25p_c$ (from dark blue to red, respectively). Critical temperature and pressure of carbon dioxide are $T_c = 304.1282$ K and $p_c = 7.3773$ MPa.

was observed in the absence of gravity, similar to measurements performed on Earth. This phenomenon is often referred to in the literature as 'critical speeding up' [12–14].

This observation is explained by the coupling of the thermal and the mechanical processes caused by thermal expansion. Since heat conduction is slow near the critical point, a thin thermal boundary layer forms in the fluid near the heated surfaces. Due to the large value of the isobaric thermal expansion coefficient, the fluid elements forming the boundary layer expand, thus inducing density and pressure variations. These disturbances propagate adiabatically through the fluid at the speed of sound [19, 20]. Consequently, the propagation of temperature at the speed of sound can also be observed, described by the acoustic wave equation

$$\frac{\partial^2 T}{\partial t^2} = a_s^2 \nabla^2 T \tag{2.4}$$

with a_s denoting the isentropic speed of sound. The acoustic propagation is characterized by the *acoustic time scale*

$$t_a = \frac{\ell}{a_s}. \tag{2.5}$$

At the critical point, the isentropic speed of sound tends to zero (for carbon dioxide calculated from the Span–Wagner equation of state [17], see the left-hand diagram of Figure 2), similarly to the thermal diffusivity. At first, it may seem paradoxical that acoustic propagation, which is considered a fundamentally fast process, also slows down in the vicinity of the critical point. However, compared to the diffusion time

scale, one can say that acoustic processes are fast if $t_\mathrm{a} \ll t_\mathrm{d}$, which is fulfilled if

$$\frac{\alpha}{a_s} \ll \ell \tag{2.6}$$

holds. As shown in the right-hand diagram of Figure 2 for carbon dioxide, the previously identified material-specific characteristic length scale $\frac{\alpha}{a_s}$ is on the order of 10^{-9} m.

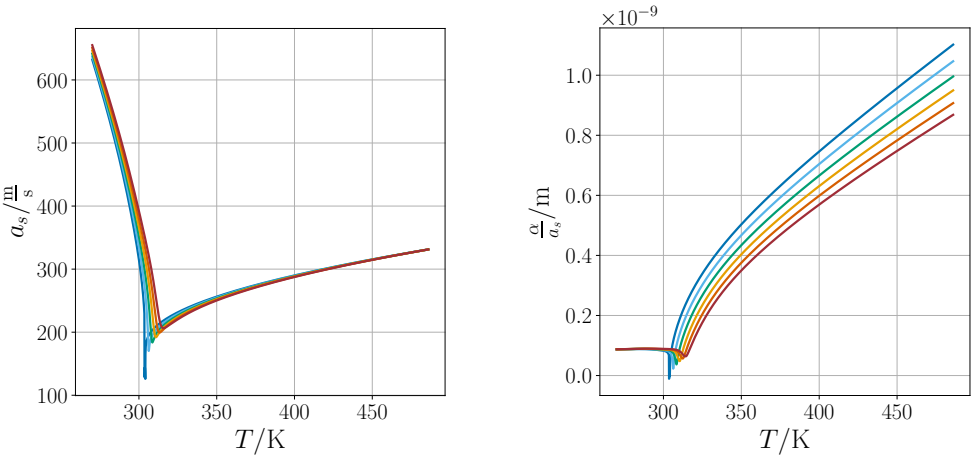

Figure 2. Temperature dependence of the isentropic speed of sound of carbon dioxide (*left*) and the material originated characteristic length scale $\frac{\alpha}{a_s}$ (*right*) along the isobaric lines $\approx 1p_\mathrm{c}$, $1.05p_\mathrm{c}$, $1.1p_\mathrm{c}$, $1.15p_\mathrm{c}$, $1.2p_\mathrm{c}$ and $1.25p_\mathrm{c}$ (from dark blue to red, respectively).

In light of our previous statements, the temperature change in a supercritical fluid can be observed practically immediately in the centimeter-sized samples used in experiments. For example, during the SpaceLab D2 mission, a series of experiments were conducted to verify the piston effect [15]. A thin-walled, spherical tank made of copper was filled with sulfur hexafluoride in a state close to its critical point. Due to the excellent thermal conductivity of copper, a homogeneous temperature rise was created on the fluid interface by heating the tank wall along a single equator with a heating filament. By ensuring spherical symmetry, the experiment could be evaluated in a single spatial dimension: temperature in the fluid was measured with thermistors at three points along the radial direction. In the experiments a heat-pulse-type excitation was applied, which means that the duration of surface heating t_p is much smaller than the diffusion time scale. However, from a technological point of view, to deliver a sufficient amount of heat, this heating time must be much longer than the acoustic time scale. This results in the suppression of acoustic processes, *i.e.,* pressure increases during the heating phase and correspondingly, the nearly isentropic temperature rise caused by the expansion of the thermal boundary layer seemingly occurs immediately without delay, implying a nearly homogeneous temperature change in

the bulk fluid. These experiments reliably confirmed the piston effect in supercritical fluids.

Although our previous argumentation essentially explains the coupling of the thermal and the mechanical processes in supercritical fluids, the usual form of the heat equation (2.2) is unable to describe such processes. Therefore, in the next subsection we briefly summarize the governing equations of coupled thermomechanical processes of fluids.

2.1. **Thermomechanical processes of fluids.** The first law of thermodynamics for a fluid element can be formulated as

$$\varrho c_p \dot{T} = -\nabla \cdot \mathbf{J}_Q + T\beta_p \dot{p} - \mathbf{\Pi} : \nabla \mathbf{v}^{\mathrm{Sym}}, \tag{2.7}$$

where ϱ, $\mathbf{v}$, $\mathbf{J}_Q$, p and $\mathbf{\Pi}$ are the density, the velocity, the heat current density, the (hydrostatic) pressure and the viscous pressure tensor, respectively [21, 22]. Furthermore, $^{\mathrm{Sym}}$ denotes the symmetric part of a second-order tensor, while the double dot product is a contraction over both indices, *i.e.,* for the tensors $\mathbf{A}$ and $\mathbf{B}$ it is defined as $\mathbf{A} : \mathbf{B} = \mathrm{tr}\left(\mathbf{A}^{\mathrm{T}}\mathbf{B}\right)$, with $^{\mathrm{T}}$ denoting the transpose and tr denoting the trace. The material time derivative

$$\dot{T} = \left(\frac{\partial}{\partial t} + \mathbf{v} \cdot \nabla\right) T \tag{2.8}$$

describes how the temperature field (as well as the pressure field) in a fixed material point changes in time, while it travels at velocity $\mathbf{v}$. Thermostatic material properties are defined by the partial derivatives of the thermal and the caloric state functions, $\varrho(T, p)$ and $h(T, p)$, respectively, with h denoting the specific enthalpy. Correspondingly, the isobaric volumetric thermal expansion coefficient β_p, the isothermal compressibility χ_T and the isobaric specific heat capacity c_p are

$$\beta_p = -\frac{1}{\varrho}\left.\frac{\partial \varrho}{\partial T}\right|_p, \qquad \chi_T = \frac{1}{\varrho}\left.\frac{\partial \varrho}{\partial p}\right|_T, \qquad c_p = \left.\frac{\partial h}{\partial T}\right|_p, \tag{2.9}$$

respectively. Thermodynamic compatibility of the thermal and the caloric equations of state is ensured through the specific entropy: when three material properties are known, then the fluid is fully characterized from a thermomechanical point of view. Thus, material properties that often arise in practical applications can be formulated as follows:

- isochoric specific heat capacity: $$c_v = c_p - \frac{T}{\varrho}\frac{\beta_p^2}{\chi_T}, \tag{2.10}$$
- heat capacity ratio: $$\gamma = \frac{c_p}{c_v} = 1 + \frac{T}{\varrho}\frac{\beta_p^2}{c_v \chi_T}, \tag{2.11}$$
- isentropic speed of sound: $$a_s = \sqrt{\frac{\gamma}{\varrho \chi_T}}. \tag{2.12}$$

Let us note here that heat capacity ratio creates further relationships, namely between the isothermal and the isentropic compressibility, as well as the isentropic and the

isothermal speed of sound, *i.e.,* $\gamma = \frac{\chi_T}{\chi_s} = \frac{a_s^2}{a_T^2}$. Internal stability of the material is ensured by the positivity of c_v and χ_T [23–25].

Usually, the heat current density and the viscous pressure are characterized by Fourier's heat conduction law and Newton's viscosity law, *i.e.,*

$$\mathbf{J}_Q = -\lambda \nabla T, \tag{2.13}$$

$$\mathbf{\Pi} = -\left(\eta_{\mathrm{Vol}} - \frac{2}{3}\eta\right)(\nabla \cdot \mathbf{v})\,\mathbf{1} - 2\eta\,(\mathbf{v} \otimes \nabla)^{\mathrm{Sym}} \tag{2.14}$$

with the thermal conductivity λ, the volume and the shear viscosities η_{Vol} and η, respectively, which all are positive due to the second law of thermodynamics.

The heat conduction equation (2.7) alone cannot describe thermal processes, as the temporal change of pressure (or density), the convective change related to the velocity field, and viscous dissipation also affect the evolution of the temperature field. Therefore, the balance equations of mass and linear momentum

$$\dot{\varrho} + \varrho \nabla \cdot \mathbf{v} = 0, \tag{2.15}$$

$$\varrho \dot{\mathbf{v}} = -\nabla p - \nabla \cdot \mathbf{\Pi} + \varrho \mathbf{g} \tag{2.16}$$

must be coupled to the heat conduction equation, where $\varrho\mathbf{g}$ represents the volumetric force field, which, for instance, originates from the gravitational field. The equations (2.7), (2.13), (2.14), (2.15) and (2.16) form a closed system, so it can be solved with appropriate initial and boundary conditions.

2.2. **Thermal equilibration model near the critical point.** Let us now focus on the microgravity experiments conducted during the SpaceLab D2 mission [15]. Due to microgravity circumstances, the volumetric force field is negligible, *i.e.,* $\varrho\mathbf{g} = \mathbf{0}$. Following [13], fluid flow can be neglected (*i.e.,* $\mathbf{v} = \mathbf{0}$) when the fast initial acoustic propagation of the disturbances is out of scope. As a consequence, the material time derivative reduces to the partial time derivative. Correspondingly, the Navier–Stokes equation (2.16) and the heat conduction equation (2.7) reduce to

$$\nabla p = 0, \tag{2.17}$$

$$\varrho c_p \frac{\partial T}{\partial t} = -\nabla \cdot \mathbf{J}_Q + T\beta_p \frac{\mathrm{d}p}{\mathrm{d}t}. \tag{2.18}$$

In light of (2.17), pressure is homogeneous during the entire process; however, it remains time dependent and can play an important role in the dynamics of the temperature field, as shown by (2.18). Let us remark here that (2.17) is already built into (2.18), since instead of $\frac{\partial p}{\partial t}$ we have written $\frac{\mathrm{d}p}{\mathrm{d}t}$. Therefore, an additional dynamical equation is required to characterize the process. Since the tank is closed during the experiment, the mass of the filled fluid remains unchanged. Neglecting the thermal expansion of the walls and applying the thermal equation of state $\varrho(T, p)$ we obtain

$$0 = \frac{\mathrm{d}m}{\mathrm{d}t} = \frac{\mathrm{d}}{\mathrm{d}t}\int\limits_{\mathcal{V}} \varrho \mathrm{d}V = \int\limits_{\mathcal{V}} \frac{\partial \varrho}{\partial t}\mathrm{d}V = \int\limits_{\mathcal{V}} \left(-\varrho\beta_p \frac{\partial T}{\partial t} + \varrho\chi_T \frac{\mathrm{d}p}{\mathrm{d}t}\right)\mathrm{d}V. \tag{2.19}$$

Due to the homogeneity of the pressure the required dynamical equation can be formulated as

$$\frac{\mathrm{d}p}{\mathrm{d}t} = \frac{\int\limits_{\mathcal{V}} \varrho \beta_p \frac{\partial T}{\partial t} \mathrm{d}V}{\int\limits_{\mathcal{V}} \varrho \chi_T \mathrm{d}V}. \tag{2.20}$$

2.3. **Thermal processes on the time scale of the heat pulse.** The heat pulse excitation achieved by electric heating can be formulated as a time-dependent boundary condition

$$\mathbf{J}_Q \cdot \mathbf{n}\big|_{\partial\mathcal{V}} = \begin{cases} \frac{\overset{*}{Q}}{A_\mathrm{s}}, & \text{if } 0 \le t \le t_\mathrm{p}, \\ 0, & \text{otherwise,} \end{cases} \tag{2.21}$$

where $\overset{*}{Q}$ represents the heating power and A_s denotes the area of the heated surface, *i.e.,* the outer surface of the spherical tank. Although spherical geometry was used in the experiments [15], our goal is to study the material behavior in the simplest possible way, so we transform spherical coordinates into Cartesian coordinates. Therefore, let us suppose a pipe with length X, which has the same volume as the spherical tank, *i.e.,* $\frac{4\pi}{3} R_\mathrm{in}^3 = AX$, with the inner radius R_in of the spherical tank and the cross section of the pipe A. In order to effectively perform the analysis in one spatial dimension, the diameter of the pipe must be negligible compared to its length, *i.e.,* $\sqrt{A} \ll X$ must hold; furthermore, all surfaces of the tube must be adiabatically insulated, except for one base circle for the duration of the heat pulse. Accordingly, the only essential direction – the axial coordinate of the pipe – is denoted by x. We do not want to modify the duration of the heat pulse and the applied heating power, *i.e.,* heat $\overset{*}{Q} t_\mathrm{p}$ is kept constant, therefore, the boundary conditions for this problem are prescribed as

$$J_Q(t, x=0) = \begin{cases} \frac{\overset{*}{Q}}{A}, & \text{if } 0 \le t \le t_\mathrm{p}, \\ 0, & \text{otherwise,} \end{cases} \qquad J_Q(t, x=X) = 0. \tag{2.22}$$

Furthermore, let us now restrict ourselves to a linear analysis in accordance with the finding of [15]. Thus, let us introduce the new variables, *i.e.,* deviation from the initial equilibrium temperature and pressure $\hat{T}(t,x) = T(t,x) - T^0$ and $\hat{p}(t) = p(t) - p^0$. Substituting (2.13) into (2.18) and linearizing it together with (2.20), we obtain the system of linearized equations

$$\varrho^0 c_p^0 \frac{\partial \hat{T}}{\partial t} = \lambda^0 \frac{\partial^2 \hat{T}}{\partial x^2} + T^0 \beta_p^0 \frac{\mathrm{d}\hat{p}}{\mathrm{d}t}, \tag{2.23}$$

$$\frac{\mathrm{d}\hat{p}}{\mathrm{d}t} = \frac{\varrho^0}{\gamma^0} \beta_p^0 \left(a_s^0\right)^2 \frac{1}{X} \int\limits_0^X \frac{\partial \hat{T}}{\partial t} \mathrm{d}x, \tag{2.24}$$

with ^{0} denoting the values of thermophysical parameters in the initial state $\left(T^0, p^0\right)$, for instance, $\varrho^0 = \varrho\left(T^0, p^0\right)$. Introducing the dimensionless time and space variables

$\tau := {}^{t}/_{t_\mathrm{p}}$ and $\xi = {}^{x}/_{X}$, equations (2.23) and (2.24) can be transformed into the form

$$\frac{\partial \hat{T}}{\partial \tau} = \frac{t_\mathrm{p}}{{}^{X^2}/_{\alpha^0}} \frac{\partial^2 \hat{T}}{\partial \xi^2} + \frac{T^0 \beta_p^0}{\varrho^0 c_p^0} \frac{\mathrm{d}\hat{p}}{\mathrm{d}\tau}, \tag{2.25}$$

$$\frac{\mathrm{d}\hat{p}}{\mathrm{d}\tau} = \frac{\varrho^0}{\gamma^0} \beta_p^0 \left(a_s^0\right)^2 \int_0^1 \frac{\partial \hat{T}}{\partial \tau} \mathrm{d}\xi. \tag{2.26}$$

Via $\gamma^0 = \frac{c_p^0}{c_v^0}$ and utilizing the constancy of the parameters, (2.26) can be rewritten as

$$\frac{\mathrm{d}\hat{p}}{\mathrm{d}\tau} = \frac{\varrho^0}{\gamma^0} \beta_p^0 \left(a_s^0\right)^2 \int_0^1 \frac{\partial \hat{T}}{\partial \tau} \mathrm{d}\xi = \frac{\beta_p^0 \left(a_s^0\right)^2}{c_p^0} \int_0^1 \varrho^0 c_v^0 \frac{\partial \hat{T}}{\partial \tau} \mathrm{d}\xi. \tag{2.27}$$

Exploiting the linearized version of the relation $\mathrm{d}u = c_v \mathrm{d}T - \frac{1}{\varrho^2}\left(T\frac{\beta_p}{\chi_T} - p\right)\mathrm{d}\varrho$ (with u denoting the specific internal energy), the above integral can be further simplified, *i.e.,*

$$\begin{aligned} \frac{\mathrm{d}\hat{p}}{\mathrm{d}\tau} &= \frac{\beta_p^0 \left(a_s^0\right)^2}{c_p^0} \int_0^1 \left(\varrho^0 \frac{\partial \hat{u}}{\partial \tau} + \frac{1}{\varrho^0} \left(T^0 \frac{\beta_p^0}{\chi_T^0} - p^0 \right) \frac{\partial \hat{\varrho}}{\partial \tau} \right) \mathrm{d}\xi \\ &= \frac{\beta_p^0 \left(a_s^0\right)^2}{c_p^0} \left(\frac{\mathrm{d}}{\mathrm{d}\tau} \int_0^1 \varrho^0 \hat{u} \mathrm{d}\xi + \frac{1}{\varrho^0} \left(T^0 \frac{\beta_p^0}{\chi_T^0} - p^0 \right) \underbrace{\int_0^1 \frac{\partial \hat{\varrho}}{\partial \tau} \mathrm{d}\xi}_{\overset{(2.19)}{=} 0} \right) = \frac{\beta_p^0 \left(a_s^0\right)^2}{c_p^0} \frac{1}{X} \frac{\mathrm{d}\hat{U}_A}{\mathrm{d}\tau}, \end{aligned} \tag{2.28}$$

with the cross-section-specific internal energy of the fluid $\hat{U}_A = \int_0^X \frac{\partial \hat{\varrho}}{\partial \tau} \mathrm{d}x$. Since volume change of the tank is zero, the first law of thermodynamics for the whole system reads

$$\frac{\mathrm{d}U}{\mathrm{d}t} = \overset{*}{Q}, \tag{2.29}$$

and if the heat capacity of the pipe wall is neglected, then

$$\frac{\mathrm{d}\hat{U}_A}{\mathrm{d}\tau} = t_\mathrm{p} \frac{\overset{*}{Q}}{A}. \tag{2.30}$$

Therefore the pressure change in the fluid can be given as

$$\frac{\mathrm{d}\hat{p}}{\mathrm{d}\tau} = \frac{\beta_p^0 \left(a_s^0\right)^2}{c_p^0} \frac{t_\mathrm{p}}{X} \frac{\overset{*}{Q}}{A}. \tag{2.31}$$

This relationship highlights that in the linear approximation, if the heating power is constant, the pressure increases linearly. Furthermore, after the heat pulse, *i.e.,* when $\overset{*}{Q} = 0$, then the pressure remains constant. The pressure after the heat pulse

is obtained via integration of (2.31) over the pulse duration t_p, *i.e.,*

$$\hat{p}\left(t_\mathrm{p}\right) = \frac{\beta_p^0 \left(a_s^0\right)^2}{c_p^0} \frac{t_\mathrm{p}}{X} \frac{\overset{*}{Q}}{A}. \tag{2.32}$$

In the first term on the r.h.s. of (2.25) the ratio of the pulse duration and the diffusion time scale $t_\mathrm{d} = {X^2}/{\alpha^0}$ appears. Since $t_\mathrm{p} \ll t_\mathrm{d}$, in the beginning of the process (*i.e.,* on the fast time scale) ${t_\mathrm{p}}/{t_\mathrm{d}} \to 0$, hence (2.25) reduces to

$$\frac{\partial \hat{T}}{\partial \tau} = \frac{T^0 \beta_p^0}{\varrho^0 c_p^0} \frac{\mathrm{d}\hat{p}}{\mathrm{d}\tau}. \tag{2.33}$$

Let us remark that the spatial derivative on the fast time scale disappears, and hence in the bulk fluid (*i.e.,* outside the thin thermal boundary layer) the governing equation effectively reduces to a spatially uniform energy balance equation under a homogeneous initial condition. Consequently, the resulting ordinary differential equation (2.33) describes the evolution of a perfectly homogeneous bulk temperature, consistent with the observed (nearly) uniform temperature rise during the heat pulse. Integrating (2.33) yields the temperature outside the boundary layer after the heat pulse:

$$\hat{T}\left(t_\mathrm{p}, x\right) = \frac{T^0}{\varrho^0} \left(\frac{\beta_p^0 a_s^0}{c_p^0}\right)^2 \frac{t_\mathrm{p}}{X} \frac{\overset{*}{Q}}{A}. \tag{2.34}$$

Let us note here that substituting (2.31) into (2.23) yields the heat conduction equation

$$\frac{\partial \hat{T}}{\partial t} = \alpha^0 \frac{\partial^2 \hat{T}}{\partial \xi^2} + \frac{T^0}{\varrho^0} \left(\frac{\beta_p^0 a_s^0}{c_p^0}\right)^2 \frac{1}{X} \frac{\overset{*}{Q}}{A}, \tag{2.35}$$

where the last term represents a homogeneous volumetric heat source. However, this equation is limited by the assumed linearity and applied boundary conditions.

Let us observe that in the linear case the pressure and the temperature changes depend only on the geometry, heating power and the initial state, which determine the values of the emerging combinations of material properties. In (2.31), exactly the nondimensional Grüneisen parameter

$$\frac{1}{\varrho} \left.\frac{\partial p}{\partial u}\right|_\varrho = \frac{\beta_p a_s^2}{c_p} \tag{2.36}$$

appears, characterizing the isochoric pressure change caused by the change of specific internal energy, while in (2.33)

$$\left.\frac{\partial T}{\partial p}\right|_s = \frac{T}{\varrho} \frac{\beta_p}{c_p} \tag{2.37}$$

emerges, describing the isentropic temperature change caused by the pressure change. However, the dynamics of the temperature on the fast time scale is governed by the product of the previous two parameters [c.f. (2.34)]. Figure 3 presents the behavior of the parameters governing the dynamics for carbon dioxide near the liquid-vapor

critical point. The Grüneisen parameter, similarly to the isentropic speed of sound and thermal diffusivity, has local minima in the vicinity of the critical point. Note that the parameter $\frac{T}{\varrho}\left(\frac{\beta_p^0 a_s^0}{c_p^0}\right)^2$ has an inflection point around the critical point and has a steep slope in this region. Accordingly, processes initiated from the same initial pressure but slightly different initial temperatures can differ greatly even in the linear case, and consequently, the temperature rise during the heat pulse can also vary intensely.

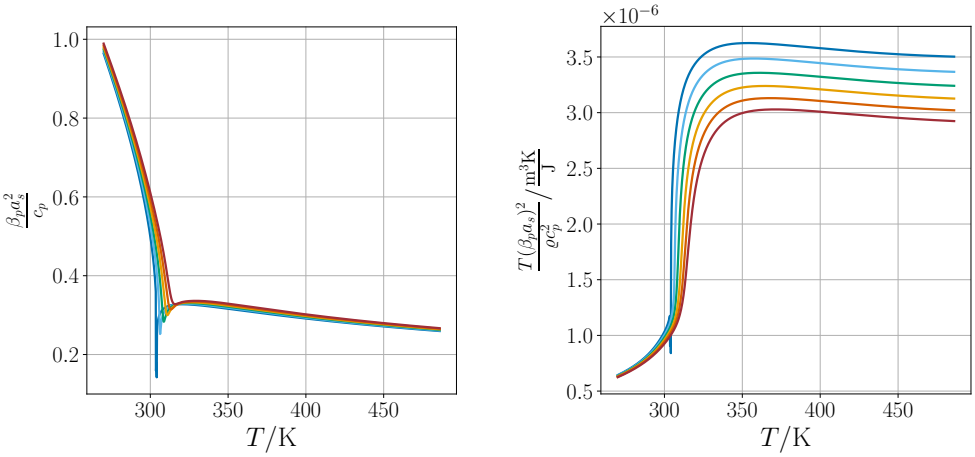

Figure 3. Temperature dependence of the parameters governing the piston effect for carbon dioxide along the isobaric lines $\approx 1p_\mathrm{c}$, $1.05p_\mathrm{c}$, $1.1p_\mathrm{c}$, $1.15p_\mathrm{c}$, $1.2p_\mathrm{c}$ and $1.25p_\mathrm{c}$ (from dark blue to red, respectively).

Finally, since the system is adiabatically insulated (except for the duration of the heat pulse) and isochoric, the temperature after homogenization can be calculated by the formula

$$\hat{T}(\infty, x) = \frac{1}{\varrho^0 c_v^0} \frac{t_\mathrm{p}}{X} \frac{\overset{*}{Q}}{A}. \tag{2.38}$$

The parameter $\frac{1}{\varrho^0 c_v^0}$ specifies the temperature change during the entire process. Its temperature dependence for carbon dioxide is presented in Figure 4.

3. An iterative numerical solution method

Although the temperature equilibration model can be simplified using linearization, heat pulse and adiabatic boundaries, for cases involving arbitrary boundary conditions and nonlinear extensions we propose a finite-difference-based approach to solve the coupled system of the pressure-corrected heat conduction equation (2.18), the pressure evolution equation (2.20), and Fourier's law (2.13).

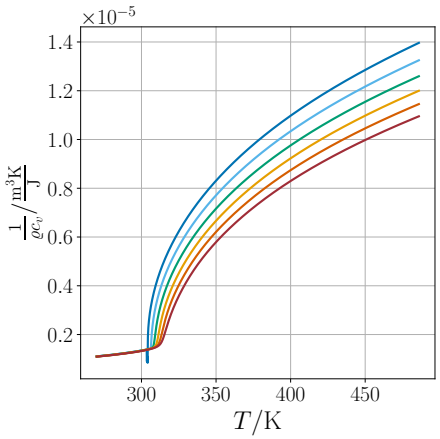

Figure 4. Temperature dependence of the parameters $\frac{1}{\varrho c_v}$ of carbon dioxide along the isobaric lines $\approx 1p_\mathrm{c}$, $1.05p_\mathrm{c}$, $1.1p_\mathrm{c}$, $1.15p_\mathrm{c}$, $1.2p_\mathrm{c}$ and $1.25p_\mathrm{c}$ (from dark blue to red, respectively).

The examined time interval is divided into equally spaced discrete time instants $t^j = j\Delta t,\ j = 0, 1, 2, \ldots$ with time step Δt, while spatial discretization is carried out on a staggered grid using equidistant cells. Temperature, as a bulk property, is located at the cell centers, while heat current density – representing inflow and outflow – is placed at the cell edges [26]. Since heat current density is prescribed at the boundaries, the one-dimensional domain $[0, X]$ can be divided into N cells with a size of $\Delta x = \frac{X}{N}$, hence $x_n = n\Delta x,\ n = 0, \ldots, N$. Accordingly, the spatial index of the heat current density is denoted via integers, while half indices are applied for the temperature, *i.e.,*

$$T\left(t^j, x_{n+1/2}\right) = T^j_{n+1/2} \qquad \text{and} \qquad J_Q\left(t^j, x_n\right) = (J_Q)^j_n\,. \tag{3.1}$$

The explicit Euler method is applied for time integration, whose stability is ensured via the choice of the time step. The stability condition of the classical heat conduction equation is $\Delta t \leq \frac{\Delta x^2}{2\alpha^0}$, which is considerably larger than t_p near the critical point. Therefore, for an appropriate resolution of the heat pulse the time step is chosen as

$$\Delta t = \min\left(\frac{\Delta x^2}{2\alpha^0}, \frac{t_\mathrm{p}}{10}\right). \tag{3.2}$$

Let us observe that both (2.18) and (2.20) contain the time derivatives of the temperature as well as of the pressure. A simple way to solve these coupled equations is to apply an iterative procedure. Correspondingly, within a single time step, first the temperature values $T^{j+1(k=0)}_{n+\frac{1}{2}}$ are determined from (2.18) without the pressure correction term. Then substituting these new values into (2.20), an estimate for the pressure $p^{j+1(k=1)}$ is determined. Subsequently, the determined pressure is substituted into (2.18), which now includes the pressure correction term and thus allows

computation of the corrected temperature values $T_{n+\frac{1}{2}}^{j+1(k=1)}$, which can be substituted into (2.20). This process continues until the difference of the temperature and pressure values between two iteration steps falls within the appropriately prescribed errors ε_T and ε_p. Thereafter, heat current density is determined from the discrete version of (2.13). The above-described iterative procedure is illustrated in Figure 5.

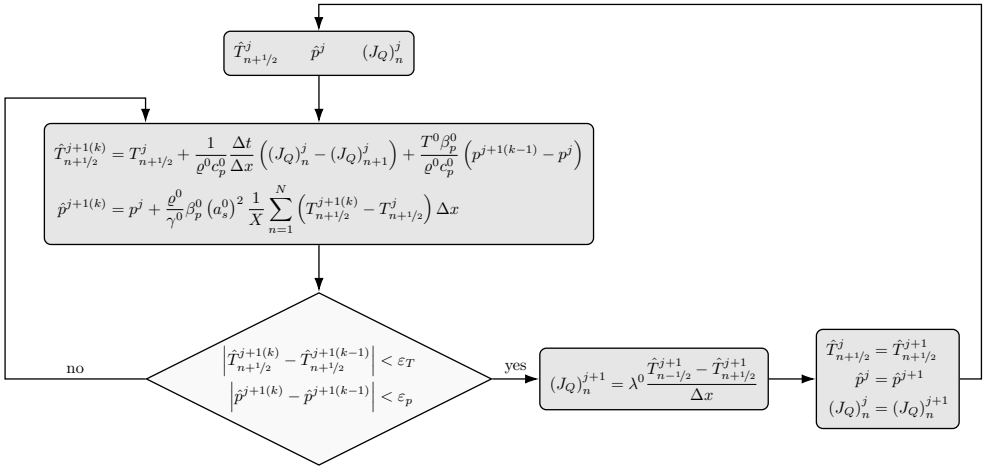

Figure 5. The iterative procedure for time integration of the governing equations

Let us note that equations (2.18), (2.20) and (2.13) are obtained neglecting the flow processes, but at this level, no linearization was applied. Therefore, the numerical scheme presented above is also applicable to investigation of material nonlinearities. Then, before the time-integration block the required material properties must be evaluated and slightly modified equations must be used for the time integration.

3.1. **Demonstration of the numerical solution.** Although sulfur hexafluoride was used in the spaceexperiment [15], carbon dioxide is used for numerical purposes. The reason for this is that high-precision, closed-form equations of state for carbon dioxide are available, which provide advantages in the planned numerical computation of the nonlinear processes. In this work, the Span–Wagner equation of state is applied, which condenses all thermostatic properties of carbon dioxide into a free energy function [17]. Thermal conductivity of the fluid is calculated using the reference correlation given by [18].

For all computations the parameters

$$R_{\text{in}} = 9.6 \text{ mm}, \qquad X = 100 \text{ mm}, \qquad \overset{*}{Q} = 3.85 \text{ mW}, \qquad t_{\text{p}} = 10 \text{ s} \tag{3.3}$$

and 100 cells along the x axis are applied, which, according to [27], provides adequate resolution for the investigation of the piston effect. All cases are computed for the duration of the diffusion time scale determined by the initial condition.

For the initial condition we have chosen $T^0 = 305$ K and $p^0 = 7.38$ MPa, accordingly, the governing parameters are $\frac{\beta_p^0 \left(a_s^0\right)^2}{c_p^0} = 0.288$, $\frac{T^0}{\varrho^0}\left(\frac{\beta_p^0 a_s^0}{c_p^0}\right)^2 = 2.32 \cdot 10^{-6}\ \frac{\mathrm{m^3K}}{\mathrm{J}}$, $\frac{1}{\varrho^0 c_v^0} = 2.57 \cdot 10^{-6}\ \frac{\mathrm{m^3K}}{\mathrm{J}}$ and $t_\mathrm{d} = 678208$ s. Table 1 presents the comparison of results obtained via the analytical formulas (2.32), (2.34) and (2.38) and via numerical simulation. The results obtained with both methods are convincing. Evolution of temperature distribution during the heat pulse is presented in Figure 6. The thermal boundary layer formed near the heated surface and the homogeneous temperature increase of the bulk fluid are clearly observed. Figure 7 shows how temperature distribution evolves after the heat pulse on the slow time scale, *i.e.,* during diffusion.

$\frac{T(t_\mathrm{p},X)-T^0}{\mathrm{K}}$		$\frac{T(\infty,x)-T^0}{\mathrm{K}}$		$\frac{p(t_\mathrm{p})-p^0}{\mathrm{Pa}}$	
analytical	numerical	analytical	numerical	analytical	numerical
0.0241	0.0241	0.0267	0.0267	2992.0	2991.4

Table 1. Comparison of analytical and numerical outcomes

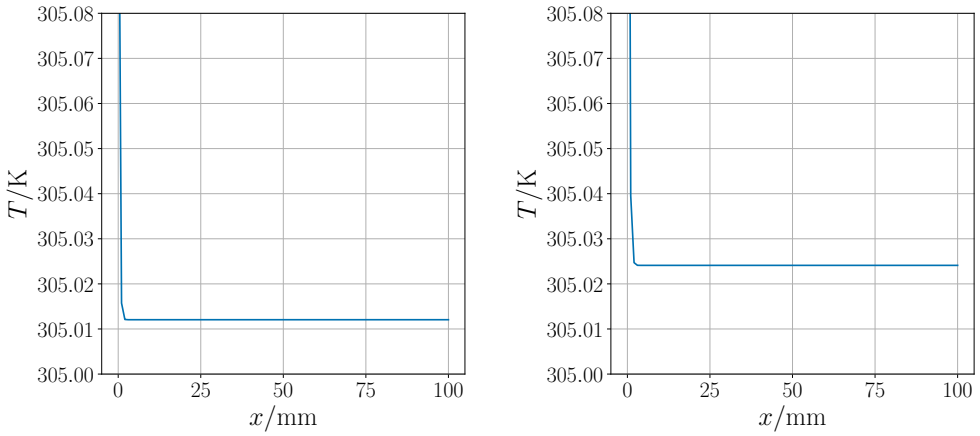

Figure 6. Temperature distribution during the heat pulse at the time instant $t = \frac{1}{2}t_\mathrm{p}$ (*left*) and at the time instant $t = t_\mathrm{p}$ (*right*)

4. Influence of initial conditions on the piston effect

Near the critical point, the governing parameters of the piston effect, similarly to the thermophysical properties, exhibit intense state dependence, as presented in Figures 3 and 4. Due to the linearization process presented above, through these governing parameters the emerging process depends on the initial state. Accordingly, in the vicinity of the critical point, relevant deviations in the solution are expected even in the linear case. In this section the sensitivity to the initial state is analyzed.

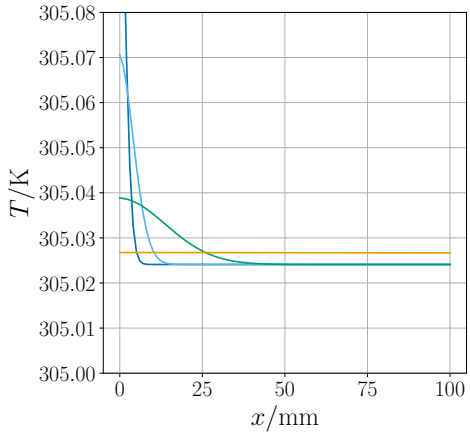

Figure 7. Temperature distribution on the diffusion time scale at the time instants $t = \frac{1}{5000}t_\mathrm{d}$, $\frac{1}{1000}t_\mathrm{d}$, $\frac{1}{100}t_\mathrm{d}$ and t_d (from dark blue to red, respectively)

4.1. **Sensitivity to initial temperature at constant initial pressure.** First, the influence of the initial temperature dependence is investigated at an unchanged initial pressure. Simulations are performed for initial temperatures $T^0 = 305$ K, 310 K, 315 K, 320 K and 325 K, while maintaining a constant initial pressure of $p^0 = 7.38$ MPa.

Figure 8 illustrates the pressure increase during the heat pulse and the initial values of its governing parameter. It can be seen that pressure rise during the process starting from the initial condition of 305 K differs significantly, whereas processes starting from the other investigated initial temperatures are nearly indistinguishable.

Similarly, Figure 9 presents the time evolution of temperature at the right boundary ($x = X$) during the heat pulse and the initial values of its governing parameter. The process starting from the initial condition of 305 K also differs significantly from the other cases.

In Figure 10, time evolution of temperature at the right boundary ($x = X$) on the diffusion time scale and initial values of the corresponding parameter are shown. The final temperature differences caused by the initial condition are obvious, as well as the harsh change of the diffusion time. The piston effect is best observed for the process starting from the initial temperature of 305 K, approximately 90 % of the temperature difference of the entire process occurs during the heat pulse, while the remaining 10 % only occurs during the incredibly long diffusion time. Moving away from the critical point, the length of the diffusion time scale normalizes and, in parallel, the temperature change occurring during the diffusion time scale accounts for an increasingly larger part of the temperature change during the entire process.

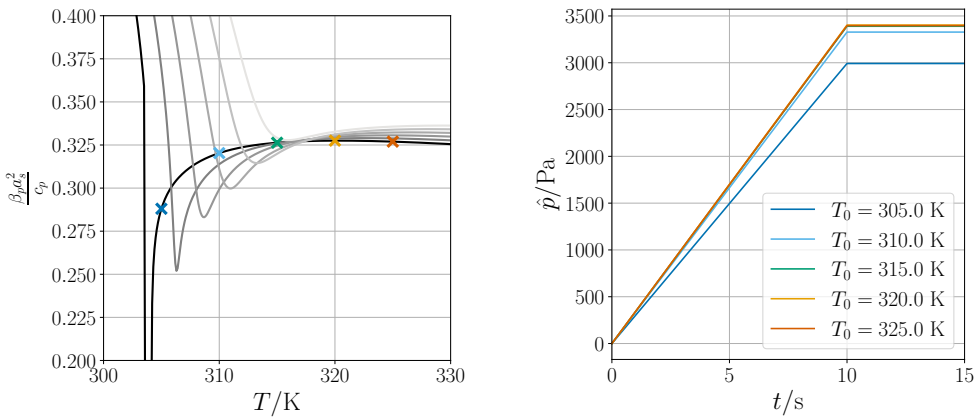

Figure 8. Influence of initial temperature on the parameter $\frac{\beta_p a_s^2}{c_p}$ (*left*) and on the time evolution of pressure increase during the heat pulse (*right*)

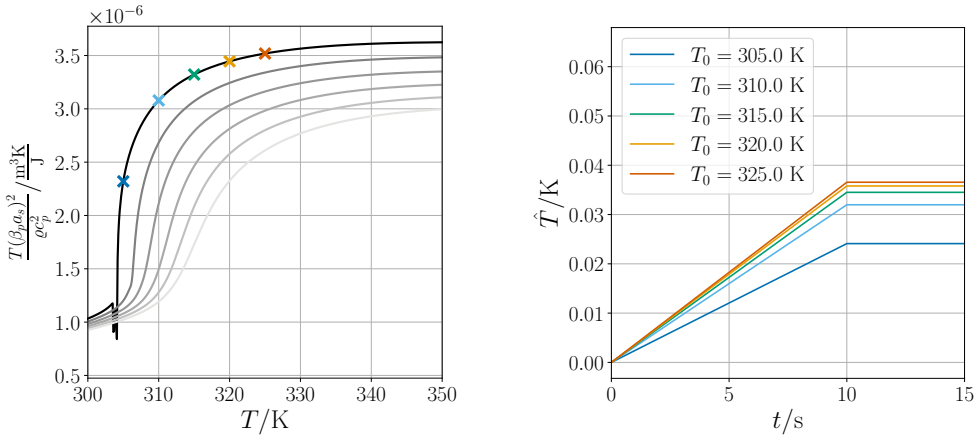

Figure 9. Influence of initial temperature on the parameter $\frac{T}{\varrho}\left(\frac{\beta_p a_s}{c_p}\right)^2$ (*left*) and on the time evolution of temperature increase at the spatial coordinate $x = X$ during the heat pulse (*right*)

4.2. **Sensitivity to initial pressure at constant initial temperature.** The influence of the initial pressure dependence is investigated at a constant initial temperature. Simulations are performed for initial pressures $p^0 = 7.38$ MPa, 7.48 MPa, 7.58 MPa, 7.68 MPa and 7.78 MPa, while maintaining a constant initial temperature of $T^0 = 305$ K. The results are presented in the same arrangement as before.

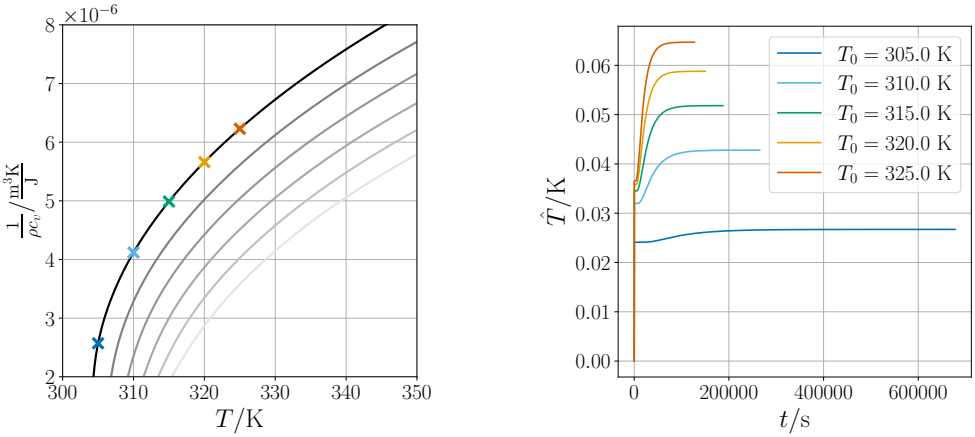

Figure 10. Influence of initial temperature on the parameter $\frac{1}{\varrho c_v}$ (*left*) and on the time evolution of temperature increase at the spatial coordinate $x = X$ on the diffusion time scale (*right*)

While in the case of increasing initial temperature, tendentious pressure and temperature increases during the heat pulse emerge, the opposite case is more hectic. The reason for this is that the governing parameters can take the same value at the same temperature but different pressures, so isobaric values of these parameters can intersect. Pressure rise and temperature rise during the heat pulse and the corresponding governing parameters are shown in Figures 11 and 12, respectively.

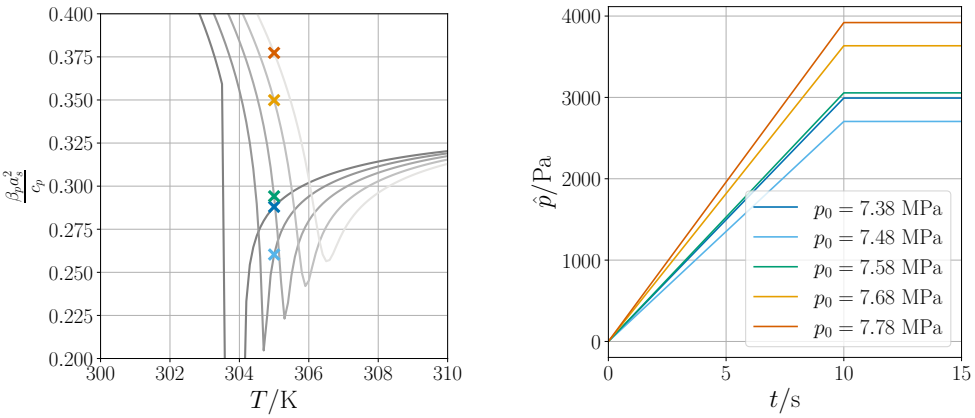

Figure 11. Influence of initial pressure on the parameter $\frac{\beta_p a_s^2}{c_p}$ (*left*) and on the time evolution of pressure increase during the heat pulse (*right*)

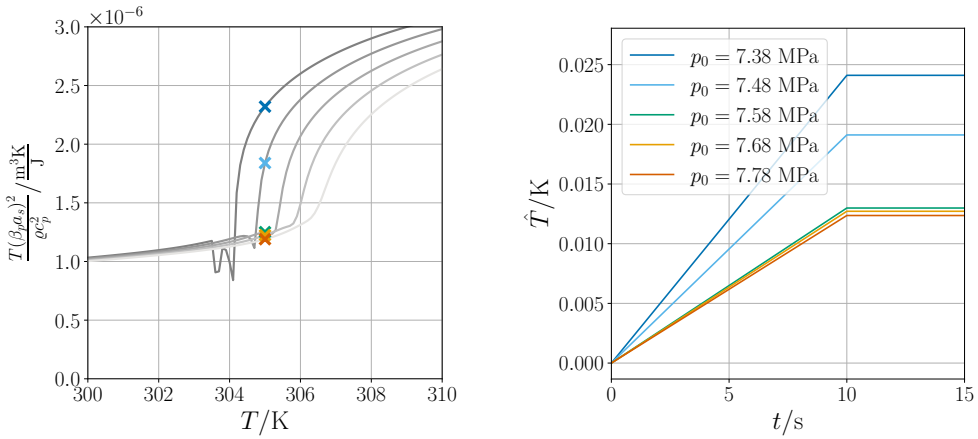

Figure 12. Influence of initial pressure on the parameter $\frac{T}{\varrho}\left(\frac{\beta_p a_s}{c_p}\right)^2$ (*left*) and on the time evolution of temperature increase at the spatial coordinate $x = X$ during the heat pulse (*right*)

Time evolution of temperature at the right boundary ($x = X$) on the diffusion time scale and initial values of the corresponding parameter are shown in Figure 13. The same digressive behavior can be observed and the piston effect can be well observed for all cases.

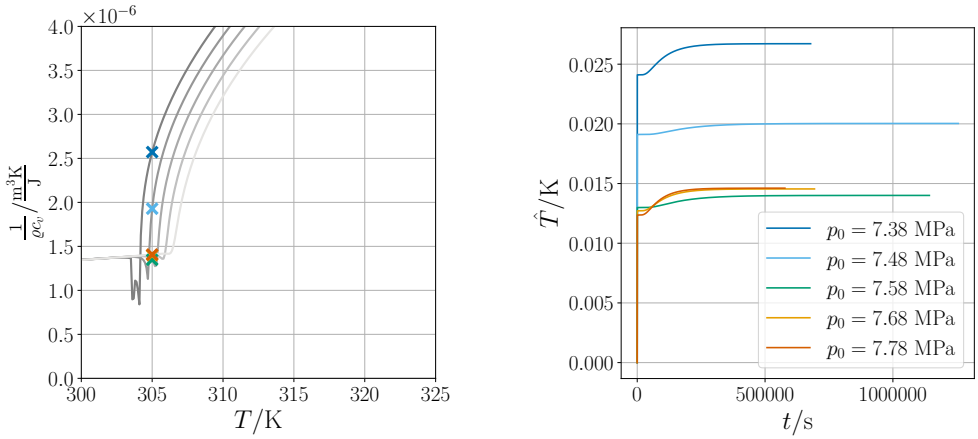

Figure 13. Influence of initial pressure on the parameter $\frac{1}{\varrho c_v}$ (*left*) and on the time evolution of temperature increase at the spatial coordinate $x = X$ on the diffusion time scale (*right*)

5. Discussion and outlook

The piston effect, a peculiar coupled thermo-mechanical phenomenon, emerges in the vicinity of the liquid–vapor critical point. Due to the exceptionally large value of the thermal expansion coefficient, pressure waves are generated in response to thermal excitation. These acoustic disturbances propagate rapidly through the fluid and lead to an apparently instantaneous temperature rise. In the heat pulse experiments the fast acoustic transients are suppressed by the long heating duration; nevertheless, the impact of the pressure on the temperature field remains essential and can be described by Boukari's thermal equilibration model, which approximation relies on a spatially homogeneous pressure field.

In this work, we have presented a detailed linear analysis of this model. On the short time scale of the heat pulse, diffusion is negligible, hence spatial derivatives vanish and the governing equations reduce to a system of ordinary differential equations. This simplified spatially homogeneous fast-time-scale limit enables an analytical approximation of the temperature and the pressure after the heat pulse. The resulting short-time-scale dynamics are controlled by two key parameters: one characterizing the isochoric pressure response to the internal-energy change (the Grüneisen parameter) and another describing the isentropic temperature change due to pressure variation. These parameters, similarly to conventional thermophysical properties, exhibit strong state dependence near the critical point. Consequently, even within the linear approximation, small variations in the initial temperature or pressure may lead to remarkable different responses. This sensitivity is confirmed by numerical simulations employing an explicit staggered-grid time-integration scheme with internal iteration. The proposed method can be straightforwardly extended to nonlinear problems in which material nonlinearities or more general boundary conditions are considered. For carbon dioxide, the influence of both the initial temperature and the initial pressure was demonstrated, and the numerical results show excellent agreement with the linear analytical predictions.

Although fluids above the critical point no longer exhibit a phase boundary, several thermophysical properties retain signatures of the liquid–vapor coexistence line in the form of extrema or inflection points. The loci of these anomalies in the supercritical region define the so-called Widom lines, which separate liquid-like and gas-like thermodynamic regimes. In contrast to the coexistence line, where many thermodynamic quantities exhibit finite jumps, each thermophysical property generally gives rise to its own Widom line. When a process crosses such a line, a qualitative change in the fluid's response may occur even without a phase transition. These features are inherited by the parameters governing the piston effect, suggesting that in the nonlinear regime further and more intricate behavior can be expected. Exploring such nonlinear thermo-mechanical interactions within the Widom region will form the basis of our future work.

6. Author contributions

K. Tóth: numerical computations, visualization, investigation of initial state dependence, manuscript text. M. Szücs: conceptualization, theoretical background, analytical calculations, supervision, manuscript text.

Acknowledgement. The research was supported by the Sustainable Development and Technologies National Programme of the Hungarian Academy of Sciences (FFT NP FTA) and by the Hungarian Scientific Research Fund under the Grant agreement NKKP STARTING24 149487.

References

[1] Akira Onuki. *Phase Transition Dynamics*. Cambridge University Press, 2002.

[2] Pierre Carlès. "A brief review of the thermophysical properties of supercritical fluids." *The Journal of Supercritical Fluids,* **53**(1), (2010), pp. 2–11. DOI: 10.1016/j.supflu.2010.02.017.

[3] Attila R. Imre, Axel Groniewsky, Gábor Györke, Adrienn Katona, and Dávid Velmovszki. "Anomalous properties of some fluids – with high relevance in energy engineering – in their pseudo-critical (Widom) region." *Periodica Polytechnica Chemical Engineering,* **63**(2), (2019), pp. 276–285. DOI: 10.3311/ppch.12905.

[4] Željko Knez, Elena Markočič, Maja Leitgeb, Mateja Primožič, M. Knez Hrnčič, and Mojca Škerget. "Industrial applications of supercritical fluids: A review." *Energy,* **77**, (2014), pp. 235–243. DOI: 10.1016/j.energy.2014.07.044.

[5] Mohammad Mizanur Rahman, Ji Dongxu, Nusrat Jahan, Massimo Salvatores, and Jiyun Zhao. "Design concepts of supercritical water-cooled reactor (SCWR) and nuclear marine vessel: A review." *Progress in Nuclear Energy,* **124**, (2020), p. 103320. DOI: 10.1016/j.pnucene.2020.103320.

[6] Pan Wu, Yanhao Ren, Min Feng, Jianqiang Shan, Yanping Huang, and Wen Yang. "A review of existing SuperCritical Water reactor concepts, safety analysis codes and safety characteristics." *Progress in Nuclear Energy,* **153**, (2022), p. 104409.

[7] Thomas Reinsch, Patrick Dobson, Hiroshi Asanuma, Ernst Huenges, Flavio Poletto, and Bernard Sanjuan. "Utilizing supercritical geothermal systems: a review of past ventures and ongoing research activities." *Geothermal Energy,* **5**(1), (2017), pp. 1–25. DOI: 10.1186/s40517-017-0075-y.

[8] Patrick Dobson, Hiroshi Asanuma, Ernst Huenges, Flavio Poletto, Thomas Reinsch, and Bernard Sanjuan. "Supercritical Geothermal Systems - A Review of Past Studies and Ongoing Research Activities." *42nd Workshop on Geothermal Reservoir Engineering.* Proceedings " 42nd Workshop on Geothermal Reservoir Engineering". Stanford, CA, United States, 2017.

[9] N. Longmire and D. T. Banuti. "Onset of heat transfer deterioration caused by pseudo-boiling in CO_2 laminar boundary layers." *International Journal of Heat and Mass Transfer,* **193**, (2022), p. 122957. DOI: 10.1016/j.ijheatmasstransfer.2022.122957.

[10] Bernard Zappoli. "Near-critical fluid hydrodynamics." *Comptes Rendus Mécanique,* **331**(10), (2003), pp. 713–726. DOI: 10.1016/j.crme.2003.05.001.

[11] Bernard Zappoli, Daniel Beysens, and Yves Garrabos. *Heat transfers and related effects in supercritical fluids.* Springer, 2015.

[12] B. Zappoli, D. Bailly, Y. Garrabos, B. Le Neindre, P. Guenoun, and D. Beysens. "Anomalous heat transport by the piston effect in supercritical fluids under zero gravity." *Physical Review A,* **41**(4),4 (1990), pp. 2264–2267. DOI: 10.1103/PhysRevA.41.2264.

[13] Hacène Boukari, J. N. Shaumeyer, Matthew E. Briggs, and Robert W. Gammon. "Critical speeding up in pure fluids." *Physical Review A,* **41**(4), (1990), p. 2260. DOI: 10.1103/PhysRevA.41.2260.

[14] Akira Onuki, Hong Hao, and Richard A Ferrell. "Fast adiabatic equilibration in a single-component fluid near the liquid-vapor critical point." *Physical Review A,* **41**(4), (1990), p. 2256. DOI: 10.1103/PhysRevA.41.2256.

[15] J. Straub, L. Eicher, and A. Haupt. "Dynamic temperature propagation in a pure fluid near its critical point observed under microgravity during the German Spacelab Mission D-2." *Physical Review E,* **51**(6), (1995), p. 5556. DOI: 10.1103/PhysRevE.51.5556.

[16] Kristóf Tóth. *A szuperkritikus dugattyúhatás kezdeti feltételektől való függésének vizsgálata (in Hungarian).* Student's Scientific Conference Thesis. 2025.

[17] Roland Span and Wolfgang Wagner. "A new equation of state for carbon dioxide covering the fluid region from the triple-point temperature to 1100 K at pressures up to 800 MPa." *Journal of physical and chemical reference data,* **25**(6), (1996), pp. 1509–1596. DOI: 10.1063/1.555991.

[18] Marcia L Huber, EA Sykioti, Marc J Assael, and Richard A Perkins. "Reference correlation of the thermal conductivity of carbon dioxide from the triple point to 1100 K and up to 200 MPa." *Journal of physical and chemical reference data,* **45**(1), (2016). DOI: https://doi.org/10.1063/1.4940892.

[19] Pierre Carlès. "Thermoacoustic waves near the liquid-vapor critical point." *Physics of Fluids,* **18**(12), (2006). DOI: 10.1063/1.2397577.

[20] Nusair Hasan and Bakhtier Farouk. "Thermoacoustic transport in supercritical fluids at near-critical and near-pseudo-critical states." *The Journal of Supercritical Fluids,* **68**, (2012), pp. 13–24. DOI: 10.1016/j.supflu.2012.04.007.

[21] Tamás Környey. *Hőátvitel (in Hungarian).* Műegyetemi Kiadó, 1999.

[22] Henning Struchtrup. *A Thermodynamic Introduction to Transport Phenomena.* Springer, 2024. DOI: 10.1007/978-3-031-61868-0.

[23] Ulrich Grigull. "Das Prinzip von Le Chatelier und Braun." *International Journal of Heat and Mass Transfer,* **7**(1), (1964), pp. 23–31.

[24] Tamás Matolcsi. *Ordinary Thermodynamics. Nonequilibrium Homogeneous Processes.* Budapest: Akadémiai Kiadó (Publishing House of the Hungarian Academy of Sciences), 2004.

[25] Adrian Bejan. *Advanced engineering thermodynamics.* John Wiley & Sons, 2016. DOI: 10.1002/9781119245964.

[26] Ágnes Rieth, Róbert Kovács, and Tamás Fülöp. "Implicit numerical schemes for generalized heat conduction equations." *International Journal of Heat and Mass*

Transfer, **126**, (2018), pp. 1177–1182. DOI: 10.1016/j.ijheatmasstransfer.2018.06.067.

[27] Donát M Takács, Tamás Fülöp, Róbert Kovács, and Mátyás Szücs. "The piston effect in supercritical fluids investigated via a reversible–irreversible vector field splitting-based explicit time integration scheme." *Physics of Fluids,* **37**(7), (2025). DOI: 10.1063/5.0271333.

Journal of Computational and Applied Mechanics, Vol. 20, No. 2, (2025), pp. 93–117
DOI: 10.32973/jcam.2025.004

THE KLUITENBERG–VERHÁS MODEL OF VISCOELASTICITY AND ITS IRREVERSIBLE THERMODYNAMICAL CONSISTENCY VIA RHEOLOGICAL ENERGY

Tamás Fülöp
Department of Energy Engineering, Faculty of Mechanical Engineering,
Budapest University of Technology and Economics
Műegyetem rkp. 3., H-1111 Budapest, Hungary;
Montavid Thermodynamic Research Group,
Society for the Unity of Science and Technology
Lovas út 18., H-1012 Budapest, Hungary
fulop.tamas@gpk.bme.hu

[Received: December 31, 2025; Accepted: March 16, 2026]

Abstract. Rocks and plastics are two examples of classes of materials where the Kluitenberg–Verhás model of viscoelasticity has proved adequate for describing the observed mechanical behaviour. This model cannot be interpreted as a generalized Maxwell model, and requires in fact a novel rheological circuit element beyond the spring and the dashpot. Moreover, its thermodynamical consistency leads to nontrivial inequality conditions on the model coefficients, ignoring which would lead to violation of the second law of thermodynamics and would thus be a principal source of instability of numerical solutions. The present paper explores the role of the rheological energy contribution embedded in the Kluitenberg–Verhás model, in a didactic and application-oriented way. The explicit meaning of the involved irreversible thermodynamical additional state variable – internal degree of freedom – is identified. Neither thermal expansion nor heat conduction is neglected, enhancing the applicability of the constructed framework.

Mathematical Subject Classification: 74A15, 76Axx, 74D05, 74L10
Keywords: viscoelasticity, internal variable, continuum theory, temporal thermodynamics

1. Introduction

Materials such as rocks and plastics do not exhibit a prompt and reversible elastic response to changes but manifest a delayed and damped behaviour. As explored by the Anelastic Strain Recovery (ASR) method [1–4], various rocks necessitate the Kluitenberg–Verhás viscoelastic model for describing the observed strain histories, and the same can be found for plastics [5]. This model adds the time derivative of stress and the first *and second* time derivatives of strain to the Hooke connection between stress and strain. Unlike the special case of Poynting–Thomson–Zener standard rheology with first stress derivative and first strain derivative, such a relationship is beyond the range of generalized Maxwell models of rheology (for a proof see, *e.g.,* [6],

Appendix A). Moreover, the Kluitenberg–Verhás model cannot be realized via the two conventional rheological circuit elements, springs and dashpots, but also demands the so-called Verhás element [7] (see Figure 1).

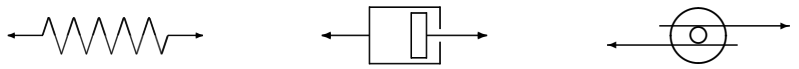

Figure 1. In addition to the two conventional rheological circuit elements, the spring (left) and the dashpot (middle), the Kluitenberg–Verhás model raises the need for a novel rheological circuit element, the Verhás element (right).

In [8], the Kluitenberg–Verhás model was derived via an additional *entropy* term, in the internal variable formalism of irreversible thermodynamics, and the inequality conditions on the model coefficiends imposed by the second law of thermodynamics have been identified and investigated.

One drawback of the treatment given in [8] is that the special case of constant model coefficients – the case most frequently demanded by concrete applications – can only be obtained in a quasi-isothermal approximation. As mentioned in [8] without any details (and considered in [9] as a forerunner to this paper), an alternative approach could be established via an additional *energy* term. Here, the latter option is worked out in detail, with unforeseen benefits: the case of constant coefficients does not require approximation of any kind, and the concrete meaning of the extra state variable – internal variable – can be revealed. This latter is particularly valuable given that, typically, the internal variable methodology cannot interpret the assumed internal variable itself but only derive its consequences on the rest, well-interpreted and measureable, quantities. Here it turns out that the rheological internal variable can be accessed as a combination of quantities that can be identified via measurement. This opens the possibility of finding analytical or numerical solutions for the whole set of state variables, including the internal variable as well. In parallel, while in [8] thermal expansion is neglected, it is not the case here. Hence, the framework presented here is suitable for applications like the ASR method of rock mechanics, which, for instance, was successfully utilized in a recent R&D project [10].

A final introductory remark is that, besides the internal-variable framework applied here, rheology utilizes various other approaches, too. Each has its virtues and limitations.

The simplest concept is that of rheological circuits. It offers a pleasant interpretation in terms of additive stresses (dynamical additivity) [realized as parallel connections] and additive strains (kinematic additivity) [realized as serial connections]. This interpretation is, however, non-unique and can thus be misleading: for example, the Poynting–Thomson–Zener model can be realized via two different three-element circuits (see, *e.g.,* [11]). Another shortcoming is that, following historical roots, only springs and dashpots are typically considered, so thermodynamically legitimate cases like the Verhás element cannot be covered.

A much more general approach is introducing history dependence using integral equations (see, for example, [12–15]). Here, one challenge is to find a suitable integral representation (cf. *e.g.,* page 310 of [13]). Another complication arises when introducing history dependence of energy and entropy (see, *e.g.,* page 78 of [14]). Finally, an integral kernel based description means infinitely many free parameters to fit from experimental data. This problematical richness is typically reduced by using prescribed patterns with a finite number of parameters, as in the form of a Prony series (cf. *e.g.,* page 315 of [15]). This introduces the limitation that, for example, the Kluitenberg–Verhás model remains out of scope (see, *e.g.,* the above-mentioned proof in Appendix A of [6]).

The internal-variable framework can also be done in an interpretation-friendlier but restrictive form when the considered internal variables are stress contributions themselves (like in [16], page 155; see also [17], page 343). This also fails to cover the Kluitenberg–Verhás model (as revealed below in the final formula of (61), where the internal variable is found to also contain a velocity gradient dependent part in addition to the nonelastic stress contribution).

When we do not bind the introduced internal variable to any particular interpretation, one drawback is the absence of any initial interpretation. On the other hand, one advantage is obtaining a model that is the most general model within that universality class. Consequently, the scene is open for any possible later interpretation – macroscopic, mesoscopic or microscopic. Fortunately, while applying the internal variable methodology, no particular interpretation is necessary: just general rules and assumptions of irreversible thermodynamics are to be followed, using mathematics only.

Moreover, in the concrete case presented in this article, even a macroscopic interpretation is found [at the already-mentioned final formula of (61)]. This enables us to identify concrete mechanisms in the future that can lead to such an additional degree of freedom.

2. The starting point

The continuum background necessary for starting is as follows (see, *e.g.,* [18]).

The velocity gradient tensor $\mathbf{L}$ is the derivative of the velocity field $\mathbf{v}$:

$$\mathbf{L} = \mathbf{v} \otimes \overleftarrow{\nabla} \qquad (\text{in Cartesian components: } L_{ij} = \partial_j \mathrm{v}_i)\,, \tag{1}$$

and the local/differential balance of internal energy is the relationship

$$\varrho \dot{e} = -\nabla \cdot \mathbf{j}_E + \mathrm{tr}\,(\boldsymbol{\sigma}\mathbf{L}) = -\nabla \cdot \mathbf{j}_E + \mathrm{tr}\left(\boldsymbol{\sigma}\mathbf{L}^{\mathsf{S}}\right) \tag{2}$$

among (mass-)specific internal energy e, heat current density $\mathbf{j}_E$, the stress tensor $\boldsymbol{\sigma}$ (assumed to be symmetric), and the symmetric part of the velocity gradient, denoted as $\mathbf{L}^{\mathsf{S}}$.[1] (Volumetric energy source is not displayed here but could be added easily

[1] In this article, a product of tensors like $\boldsymbol{\sigma}\mathbf{L}$ denotes the composition of linear maps, hence, in Cartesian indices, $(\boldsymbol{\sigma}\mathbf{L})_{kl} = \sigma_{km} L_{ml}$. Another popular convention is to write this as $\boldsymbol{\sigma} \cdot \mathbf{L}$.

[19].) The local/differential balance of entropy is the connection

$$\varrho\dot{s} = -\nabla\cdot\mathbf{j}_S + \pi_S \tag{3}$$

between specific entropy s, entropy current density $\mathbf{j}_S$, and entropy production rate density π_S. Between entropy current density and heat current density, we consider the customary relationship

$$\mathbf{j}_S = \frac{1}{T}\mathbf{j}_E\,, \tag{4}$$

where $T > 0$ is absolute temperature.

In case of a reversible model,

$$\pi_S = 0 \tag{5}$$

along any allowed process, while for an irreversible model we investigate the inequality

$$\pi_S \geq 0 \tag{6}$$

as dictated by the second law of thermodynamics.

Heat conduction is going to be incorporated in Sect. 13; before that, in order to help focus on the mechanical irreversibility, we "switch heat conduction off":

$$\mathbf{j}_E = \mathbf{0}, \quad \mathbf{j}_S = \mathbf{0}\,. \tag{7}$$

Then, for a reversible model,

$$T\pi_S = 0, \tag{8}$$

require

$$T\pi_S = \varrho T\dot{s} \geq 0\,. \tag{9}$$

As a remark, the form $\mathrm{tr}\,(\boldsymbol{\sigma}\mathbf{L})$ of mechanical power density enables the forthcoming considerations to be applicable not only for continuum theory but also for the space-independent/homogeneous (also called lumped/concentrated-parameter) description, in other words, temporal thermodynamics [18, 20, 21]. Namely, no space derivatives appear hereafter, and $\mathbf{L}^{\mathsf{S}}$ may also be treated as a degree of freedom in its own right, not only as a space derivative of some other degree of freedom. Its connection to other kinematic quantities may be derived not only from the continuum perspective [22–27] but can also be postulated (still motivated by the continuum description, naturally). Therefore, we can obtain a space-independent, finite degree-of-freedom, temporal dynamical model for elastic, viscoelastic, and thermal-expansion phenomena. This is a practically simple framework that is satisfactory for discussing a class of experimental setups (such as those mentioned in the Introduction regarding rocks and plastics).

We are closer to engineering practice if our thermal state variable is T rather than e or s. First, let us allow for thermal changes only:

$$e = e_{\mathrm{th}}(T), \quad s = s_{\mathrm{th}}(T), \tag{10}$$

among which the Gibbs relation

$$\mathrm{d}e = T\,\mathrm{d}s \tag{11}$$

(as a constitutive consistency condition) is ensured by imposing

$$\frac{\mathrm{d}e_{\mathrm{th}}}{\mathrm{d}T} = T\frac{\mathrm{d}s_{\mathrm{th}}}{\mathrm{d}T}\,. \tag{12}$$

[In the language of the variable T, concavity of $s(e)$ can be expressed as $\mathrm{d}e_{\mathrm{th}}/\mathrm{d}T > 0$, or, equivalently, $\mathrm{d}s_{\mathrm{th}}/\mathrm{d}T > 0$.] In particular,

$$e_{\mathrm{th}}(T) = cT, \qquad s_{\mathrm{th}}(T) = c\ln\frac{T}{T_{\mathrm{ref}}} + s_{\mathrm{ref}} \tag{13}$$

embodies a model with constant specific heat capacity c (here, s_{ref} denotes the value of s at an arbitrarily chosen reference temperature value T_{ref}.)

In addition to thermal changes, we are going to introduce elastic, viscoelastic and thermal-expansion phenomena gradually.

We restrict ourselves to small deformations of an isotropic material. In this approximation, mass density ϱ is constant.

We are going to have elastic and thermal-expansion deformations. Elastic deviation is measured locally and tensorially by the elastic deformedness tensor $\mathbf{D}$ – the full details[2] on the kinematic-type state quantity $\mathbf{D}$ and its relationship to $\mathbf{L}$ and the customarily used strain tensor $\boldsymbol{\varepsilon}$ can be found in [18, 22–27]. Even in small-$\mathbf{D}$ approximation elasticity, $\boldsymbol{\varepsilon} \not\equiv \mathbf{D}$ but $\boldsymbol{\varepsilon} = \mathbf{D} - \mathbf{D}_{\mathrm{initial}}$. Unlike it is done customarily, we do not assume $\mathbf{D}_{\mathrm{initial}} = \mathbf{0}$, *i.e.,* that the process starts from an undeformed state. This is particularly important for applications like the above-mentioned ASR method of rock mechanics, where the sample is initially in a compressed underground state. Accordingly, strain is not a thermodynamical state quantity but a change quantity, like heat and work. The elasticity-related thermodynamical state quantity is $\mathbf{D}$. Later [in formula (71) below] we will see that, while $\dot{\boldsymbol{\varepsilon}} = \mathbf{L}^{\mathsf{S}}$ is only a gross kinematic change rate, the thermodynamical state quantities $\mathbf{D}$ and T enable its decomposition into elastic and thermal-expansion change rates.

Regarding thermal expansion, the thermal expansion coefficient is assumed constant. Its temperature dependence would make even the small-deformation treatment nonlinear. Fortunately, for a large range of practical applications, the contribution of this higher-order effect would be very small.[3] On the other side, a constant but *nonzero* thermal expansion coefficient is important to consider. Its role has been found remarkable, for example, in the ASR method. Hence, in the ASR protocol, either air conditioning in a sealed room or a water or oil bath with a circulator is

[2] As a brief summary, at a material point on the material manifold, the instantaneous metric tensor $\mathbf{h}$ is the realized metric at an instant (providing the instantaneous distances between material points), while the relaxed metric tensor $\mathbf{g}$ is the metric the solid takes when being in a stressless relaxed state. The elastic deformedness tensor $\mathbf{D} = \ln\sqrt{\mathbf{g}^{-1}\mathbf{h}}$ measures the deviation between these two metrics. If $\mathbf{h} \approx \mathbf{g}$ then $\mathbf{D}$ is small ($\|\mathbf{D}\| \ll 1$). The time evolution of $\mathbf{D}$ is determined by the time evolution of $\mathbf{h}$ (which is of purely kinematic origin), while, for pure elasticity, $\mathbf{g}$ is constant, leading for small $\mathbf{D}$ to $\dot{\mathbf{D}} \approx \mathbf{L}^{\mathsf{S}} = \dot{\boldsymbol{\varepsilon}} \Rightarrow \mathbf{D} - \mathbf{D}_{\mathrm{initial}} = \boldsymbol{\varepsilon}$ via time integration (as $\boldsymbol{\varepsilon}_{\mathrm{initial}} = \mathbf{0}$ by definition). Thermal expansion is manifested in nonconstant, T-dependent, $\mathbf{g}$, and time-dependent T leads to time-dependent $\mathbf{g}$; theű analogous time integration for small deformations reveals an additive thermal expansion-related contribution in $\boldsymbol{\varepsilon}$.

[3] As an example, in the comprehensive book [28] on thermal stresses induced by thermal expansion, it is hard to find any mentioning of temperature dependence of the thermal expansion coefficient.

applied to keep the temperature of the measured sample as constant as possible [1–4]. In addition, they found it necessary to add a dummy specimen, which does not undergo any deformation except thermal expansion, for monitoring the deformation due to the remaining unavoidable (1−2) °C temperature fluctuation.

In order to focus on the thermodynamical aspects, first let us consider one space dimension – more properly, one kinematic degree of freedom. Note that such a treatment is not for uniaxial processes: that would be a self-deception because transversal changes are hardwired to the longitudinal ones – via Poisson's ratio – only for pure elasticity; rheology makes the transversal changes decouple from the longitudinal ones, see, *e.g.,* [18]. Instead, for isotropic materials, the deviatoric and spherical parts of the model both prove to be effectively scalar (o)ne kinematic degree of freedom type. Between the two parts, the spherical (volumetric) part will contain isotropic thermal expansion. The details will follow below. The full tensorial treatment of isotropic materials begins in Sect. 12.

3. The Hooke model

Elasticity is actually a reversible internal-variable extension of the above thermal-only model (10)–(12).

Namely, in addition to T and the related aspects (10)–(12), we consider an extra degree of freedom D. It plays a kinematic role, which will be expressed by its relationship to L as

$$\dot{D} = L\,. \tag{14}$$

Let stress, σ, be the linear function

$$\sigma = ED \tag{15}$$

of this state variable, with the positive coefficient E (which, in case of uniaxial interpretation, is Young's modulus). The mechanical power density σL of this stress is reversible and nondissipative if specific internal energy is shifted in the following quadratic convex way:

$$e(T,D) = e_{\mathrm{th}}(T) + \frac{E}{2\varrho}D^2 \tag{16}$$

[following from which $s(e,D)$ proves concave]. In the meantime, specific entropy is not shifted and is kept D-independent:

$$s = s_{\mathrm{th}}(T)\,. \tag{17}$$

Then

$$\begin{aligned} T\pi_S = \varrho T\dot{s} = \varrho T\frac{\mathrm{d}s_{\mathrm{th}}}{\mathrm{d}T}\dot{T} = \varrho\frac{\mathrm{d}e_{\mathrm{th}}}{\mathrm{d}T}\dot{T} = \varrho\dot{e}_{\mathrm{th}} = \varrho\left(e - \frac{E}{2\varrho}D^2\right)^{\cdot} = \varrho\dot{e} - ED\dot{D} = \\ = \sigma L - ED\dot{D} = \sigma\dot{D} - ED\dot{D} = (\sigma - ED)\dot{D} = 0\,. \end{aligned} \tag{18}$$

Meanwhile, temperature proves constant since, according to (18), along any allowed process

$$\dot{e}_{\mathrm{th}} = 0, \tag{19}$$

thus

$$0 = \dot{e}_{\mathrm{th}} = \frac{\mathrm{d}e_{\mathrm{th}}}{\mathrm{d}T}\dot{T}, \tag{20}$$

which, in light of $\frac{\mathrm{d}e_{\mathrm{th}}}{\mathrm{d}T} > 0$ (see above) leads to

$$\dot{T} = 0\,. \tag{21}$$

Hence, the model is reversible (*i.e.,* no entropy production) and nondissipative (*i.e.,* no change in $T \Rightarrow$ no change in the thermal term $e_{\mathrm{th}} \Rightarrow$ mechanical power modifies the elastic term $\frac{E}{2\varrho}D^2$ only $\Rightarrow$ no conversion of mechanical energy into thermal).

4. The Kelvin–Voigt model

Compared to the previous elastic model, let e and s remain unmodified. However, let an extra – viscosity-type – term be present in stress:

$$\sigma = ED + \hat{E}L = ED + \hat{E}\dot{D}\,, \tag{22}$$

with viscosity coefficient $\hat{E}$.[4]

This is the Kelvin–Voigt model. With the irreversible stress contribution

$$\hat{\sigma} = \sigma - ED\,, \tag{23}$$

which is now

$$\hat{\sigma} = \hat{E}\dot{D}\,, \tag{24}$$

$$\begin{aligned} T\pi_S = \varrho T\dot{s} = \varrho T\frac{\mathrm{d}s_{\mathrm{th}}}{\mathrm{d}T}\dot{T} = \varrho\frac{\mathrm{d}e_{\mathrm{th}}}{\mathrm{d}T}\dot{T} = \varrho\dot{e}_{\mathrm{th}} = \varrho\left(e - \frac{E}{2\varrho}D^2\right)^{\cdot} = \varrho\dot{e} - ED\dot{D} = \\ = \sigma L - ED\dot{D} = \sigma\dot{D} - ED\dot{D} = \hat{\sigma}\dot{D} + ED\dot{D} - ED\dot{D} = \hat{E}\dot{D}^2 \geq 0 \end{aligned} \tag{25}$$

so the model is irreversible ($\hat{E} < 0$ is excluded by the second law of thermodynamics). In parallel, temperature increases (r decreases) monotonously (:)

$$\varrho\frac{\mathrm{d}e_{\mathrm{th}}}{\mathrm{d}T}\dot{T} = \varrho\dot{e}_{\mathrm{th}} = \hat{E}\dot{D}^2 \geq 0\,. \tag{26}$$

Let us also observe the relationship

$$T\pi_S = \hat{\sigma}\dot{D} = \hat{\sigma}L \tag{27}$$

because we find similar formulae below.

[4]The coefficient combination $\hat{E}/E$ is a time scale, and turns out to be the characteristic time for creep (which is when $\sigma = \mathrm{const.}$, hence, D increases in time exponentially towards the corresponding Hooke prediction σ/E).

5. The Poynting–Thomson–Zener model

For the purpose of the Poynting–Thomson–Zener (PTZ) model[5]

$$\sigma + \tau\dot{\sigma} = ED + \hat{E}L \qquad \text{or} \qquad \sigma + \tau\dot{\sigma} = ED + \hat{E}\dot{D}\,, \tag{28}$$

a new degree of freedom introducing irreversibility is needed. In paper [8] specific entropy is shifted by a term proportional to the square of the new degree of freedom ξ: temporarily switching to their notations,

$$\tilde{s}(e, D, \xi) = s(e, D) - \frac{1}{2}\xi^2\,, \tag{29}$$

while they do not modify e. This, however, is approximately the same as if we leave specific entropy unmodified but shift specific internal energy by a quadratic term of ξ:

$$e(\tilde{s}, D) = e\left(s + \tfrac{1}{2}\xi^2, D\right) \approx e(s, D) + \tfrac{\partial e}{\partial s}\big|_D \cdot \tfrac{1}{2}\xi^2 = e + T \cdot \tfrac{1}{2}\xi^2\,. \tag{30}$$

Here, we choose to shift specific internal energy by an extra term and keep s unmodified.[6]

In case of the PTZ model we can find the appropriate extra term "by hand". As the first step, let us rewrite (28) (in its second variant) with the aid of (23):

$$(\hat{\sigma} + ED) + \tau(\hat{\sigma} + ED)^{\cdot} = ED + \hat{E}\dot{D}\,, \tag{31}$$

$$\hat{\sigma} + \tau\dot{\hat{\sigma}} = \left(\hat{E} - \tau E\right)\dot{D} = \hat{I}\dot{D}, \tag{32}$$

where

$$\hat{I} := \hat{E} - \tau E \tag{33}$$

(named the *index of damping*). Both convexity of e (concavity of s) and positive definiteness of π_S excludes $\hat{I} < 0$ [see (36)], and $\hat{I} = 0$ means a redundant resonant [29] case: (28) is then Hooke's law (15) plus its time derivative multiplied by τ. Therefore, a meaningful PTZ model has $\hat{I} > 0$ (which we assume hereafter).

Next, let us consider the balance of internal energy:

$$\varrho\dot{e} = \sigma L = \sigma\dot{D} = ED\dot{D} + \hat{\sigma}\dot{D} = \left(\frac{E}{2}D^2\right)^{\cdot} + \hat{\sigma}\left[\frac{1}{\hat{I}}\left(\hat{\sigma} + \tau\dot{\hat{\sigma}}\right)\right] =$$

$$= \left(\frac{E}{2}D^2 + \frac{\tau}{2\hat{I}}\hat{\sigma}^2\right)^{\cdot} + \frac{\hat{\sigma}^2}{\hat{I}}\,. \tag{34}$$

[5]The coefficient τ is a time scale, and turns out to be the characteristic time for stress relaxation (which is when D = const., hence, σ decreases in time exponentially towards the corresponding Hooke prediction ED).

[6]Assuming a new term in s or e in the internal-variable approach is a step corresponding to assuming a new stress contribution. Thermodynamical consistency requires it so that the resulting generalized model will be thermodynamically correct. *Interpreting* such a new term may be possible when the corresponding internal variable gets an interpretation. For complex materials like rocks the interpretation may be difficult; nevertheless, the model as an effective description can be valuable: just a few new parameters fitted from experiments can provide a reliable and efficient modeling of the time-dependent and irreversible processes of that complex material.

This points out that if

$$e = e_{\mathrm{th}} + \frac{E}{2\varrho} D^2 + \frac{\tau}{2\varrho \hat{I}} \hat{\sigma}^2 \tag{35}$$

is our specific internal energy then, analogously to what we have seen above,

$$\begin{aligned} T\pi_S = \cdots = \varrho \dot{e}_{\mathrm{th}} = \varrho \left[\dot{e} - \left(\frac{E}{2\varrho} D^2 + \frac{\tau}{2\varrho \hat{I}} \hat{\sigma}^2 \right)^{\cdot} \right] = \\ = \left(\frac{E}{2} D^2 + \frac{\tau}{2\hat{I}} \hat{\sigma}^2 \right)^{\cdot} + \frac{\hat{\sigma}^2}{\hat{I}} - \varrho \left(\frac{E}{2} D^2 + \frac{\tau}{2\hat{I}} \hat{\sigma}^2 \right)^{\cdot} = \frac{\hat{\sigma}^2}{\hat{I}} \geq 0 , \end{aligned} \tag{36}$$

i.e., we have obtained a model with positive definite entropy production rate density in consistency with the second law of thermodynamics.

In parallel, also analogously, the time dependence of temperature is monotonously nondecreasing again:

$$\varrho \frac{\mathrm{d}e_{\mathrm{th}}}{\mathrm{d}T} \dot{T} = \varrho \dot{e}_{\mathrm{th}} = \frac{\hat{\sigma}^2}{\hat{I}} \geq 0 . \tag{37}$$

Therefore, in case of the PTZ model, the extra internal variable has been obtained directly: the beyond-Hooke stress contribution $\hat{\sigma}$ itself plays this role.

6. The inertial Hooke model

Also still as a preparatory phase, let us now try to find the appropriate shift of specific internal energy for a doubly incomplete Kluitenberg–Verhás model – the inertial Hooke model –

$$\sigma = ED + \hat{\hat{E}} \ddot{D} : \tag{38}$$

now the beyond-Hooke stress contribution is[7]

$$\hat{\sigma} = \hat{\hat{E}} \ddot{D} \tag{39}$$

and, based on

$$\varrho \dot{e} = \sigma \dot{D} = ED\dot{D} + \hat{\sigma} \dot{D} = \left(\frac{E}{2} D^2 + \frac{\hat{\hat{E}}}{2} \dot{D}^2 \right)^{\cdot} , \tag{40}$$

having

$$e = e_{\mathrm{th}} + \frac{E}{2\varrho} D^2 + \frac{\hat{\hat{E}}}{2\varrho} \dot{D}^2 \tag{41}$$

[7]This rheological term describes an inertia-type effect coming possibly from a mesoscopic or microscopic level (for instance, micro-translations or micro-rotations), appearing macroscopically with a coefficient $\hat{\hat{E}}$. This is the effect that requires introducing the Verhás element (see Figure 1). Probably because of its conceptual novelty, this element is not yet a typical target for experimental or microscopic/mesoscopic justifications, although related ideas supporting this go back to [30].

gives

$$T\pi_S = \cdots = \varrho\dot{e}_{\mathrm{th}} = \varrho\left[\dot{e} - \left(\frac{E}{2\varrho}D^2 + \frac{\hat{\hat{E}}}{2\varrho}\dot{D}^2\right)^{\cdot}\right] = 0\,, \tag{42}$$

that is, the model is reversible and the temperature is constant.

For future benefit, it is worth rewriting (41) as

$$e = e_{\mathrm{th}} + \frac{E}{2\varrho}D^2 + \frac{1}{2\varrho\hat{\hat{E}}}\left(\hat{\hat{E}}L\right)^2 \tag{43}$$

– the benefit of this will turn out later.

Note that, in this case, not $\hat{\sigma}$ but L plays the role of the extra degree of freedom. The two cases seem to have nothing in common. This is a puzzling situation. (A synthesis will arrive, nevertheless, in Sect. 8.)

7. The relaxation-free Kluitenberg–Verhás model

Adding to the previous model (38) the Kelvin–Voigt viscous stress term results in the relaxation-free Kluitenberg–Verhás model

$$\sigma = ED + \hat{E}\dot{D} + \hat{\hat{E}}\ddot{D}\,, \tag{44}$$

in which case the same specific internal energy

$$e = e_{\mathrm{th}} + \frac{E}{2\varrho}D^2 + \frac{\hat{\hat{E}}}{2\varrho}\dot{D}^2, \qquad \text{or} \qquad e_{\mathrm{th}} + \frac{E}{2\varrho}D^2 + \frac{1}{2\varrho\hat{\hat{E}}}\left(\hat{\hat{E}}L\right)^2 \tag{45}$$

yields, again analogously,

$$T\pi_S = \cdots = \varrho\dot{e}_{\mathrm{th}} = \cdots = \hat{E}\dot{D}^2 \geq 0. \tag{46}$$

so both irreversibility and the time dependence of temperature agree with what we have seen for the Kelvin–Voigt model.

8. The full Kluitenberg–Verhás model

After our successes with all the special subfamilies, it may be surprising (and probably disappointing) that no similar direct construction is viable for the full Kluitenberg–Verhás model, that is, for

$$\sigma + \tau\dot{\sigma} = ED + \hat{E}\dot{D} + \hat{\hat{E}}\ddot{D} \tag{47}$$

with all coefficients being nonzero. Looking back from the end of this Section, this is no wonder: the full Kluitenberg–Verhás model carries a richness that is not present in any of the subfamilies. Instead of trying to find the thermodynamical model around (47), let us adapt the methodology seen in [8] but, here, use it for shifting specific internal energy rather than specific entropy.

Accordingly, let us now proceed in the opposite direction, where (47) is not an input but an output; our initial demand is only that

$$\hat{\sigma} \equiv \sigma - ED \tag{48}$$

(the rheological stress contribution) should be nonzero.

Let us shift the Hooke-level specific internal energy (16) by a term depending on a – yet uninterpreted – extra internal variable η. In order to maintain convexity (and thus concavity of s), the simplest choice to try is

$$e(T, D, \eta) = e_{\mathrm{th}}(T) + \frac{E}{2\varrho} D^2 + \frac{\kappa}{2\varrho} \eta^2 \tag{49}$$

with a non-negative κ that could in general be dependent on the state variables but here, aiming for a model practical for applications, we wish it to be constant.

As in the earlier cases, we do not modify specific entropy. In addition, let L still be equal to $\dot{D}$ [cf. (14)] (thus thermal expansion is still neglected, until Sect. 10). Accordingly, we can proceed analogously as before:

$$\begin{aligned} T\pi_S = \cdots = \varrho \dot{e}_{\mathrm{th}} = \varrho \left[\dot{e} - \left(\frac{E}{2\varrho} D^2 + \frac{\kappa}{2\varrho} \eta^2 \right)^{\cdot} \right] = \sigma L - ED\dot{D} - \kappa \eta \dot{\eta} = \\ = \hat{\sigma} L + EDL - ED\dot{D} - \kappa \eta \dot{\eta} = \hat{\sigma} L - \kappa \eta \dot{\eta} \,. \end{aligned} \tag{50}$$

The resulting expression is not *ab ovo* positive definite – let us ensure its positive definiteness choosing Onsagerian equations in our model, in the following form:

$$\hat{\sigma} = \mu_{11} L + \mu_{12} \kappa \dot{\eta} \,, \tag{51}$$

$$-\eta = \mu_{21} L + \mu_{22} \kappa \dot{\eta} \,, \tag{52}$$

and let us restrict ourselves to constant Onsagerian coefficients μ_{11}, μ_{12}, μ_{21}, μ_{22}. The rightmost-hand side of (50) is then positive definite if and only if the symmetric part of the 2×2 matrix μ (*i.e.,* μ^{S}) is positive definite, which is equivalent (see, *e.g.,* [8, 18]) to the set of conditions

$$\mu_{11} \geq 0 \,, \qquad \mu_{22} \geq 0 \,, \qquad \mu_{11}\mu_{22} - \left(\frac{\mu_{12} + \mu_{21}}{2} \right)^2 \geq 0 \,. \tag{53}$$

Let us eliminate the internal variable η: first, let us rewrite (52) into

$$-\left(1 + \mu_{22} \kappa \partial_t\right) \eta = \mu_{21} L \,, \tag{54}$$

let us act by the here-recognized differential operator $1 + \mu_{22}\kappa\partial_t$ on (51):

$$\begin{aligned} \hat{\sigma} + \underbrace{\mu_{22}\kappa}_{=:\tau} \dot{\hat{\sigma}} = \underbrace{\mu_{11}}_{=:\hat{I}} L + \mu_{11}\mu_{22}\kappa \dot{L} + \left(1 + \mu_{22}\kappa\partial_t\right) \mu_{12} \kappa \partial_t \eta = \\ = \hat{I} L + \kappa \mu_{11}\mu_{22} \dot{L} + \mu_{12} \kappa \partial_t \left(1 + \mu_{22}\kappa\partial_t\right) \eta = \\ = \hat{I} L + \kappa \mu_{11}\mu_{22} \dot{L} + \mu_{12} \kappa \partial_t \left[-\mu_{21} L\right] = \hat{I} L + \underbrace{\kappa \det \mu}_{=:\hat{\hat{E}}} \dot{L} \,, \end{aligned} \tag{55}$$

and substituting (48) (and applying $L = \dot{D}$ for combining two terms and rewriting a further term) the result is of the form (47):

$$\sigma - ED + \tau\left(\dot{\sigma} - E\dot{D}\right) = \hat{I}\dot{D} + \hat{\hat{E}}\ddot{D}\,, \tag{56}$$

$$\sigma + \tau\dot{\sigma} = ED + \big(\underbrace{\hat{I} + \tau E}_{=:\hat{E}}\big)\,\dot{D} + \hat{\hat{E}}\ddot{D}\,. \tag{57}$$

For the coefficients appearing here, we find in virtue of (53)

$$\hat{I} \geq 0\,, \qquad \tau \geq 0\,, \qquad \hat{E} \geq \tau E \tag{58}$$

and, as consequence of

$$0 \leq \mu_{11}\mu_{22} - \left(\frac{\mu_{12}+\mu_{21}}{2}\right)^2 = \mu_{11}\mu_{22} - \frac{\mu_{12}^2}{4} - \frac{\mu_{12}\mu_{21}}{2} - \frac{\mu_{21}^2}{4} =$$

$$= \det\mu - \left(\frac{\mu_{12}-\mu_{21}}{2}\right)^2 \leq \det\mu\,, \tag{59}$$

$$\hat{\hat{E}} \geq 0\,. \tag{60}$$

Inspecting equations (51)–(52), we can see that, for $\mu_{12} = 0$, (51) establishes a Kelvin–Voigt relationship between $\hat{\sigma}$ and L, while η is decoupled. We have seen previously that the Kelvin–Voigt case does not require a rheological extra energy term. (Even if there were an extra energy term, the Kelvin–Voigt mechanics would not make it change in time so it would be a "sleeping", irrelevant energy type.) Here, we are interested in the thermodynamically consistent background behind the beyond-Hooke stress contribution so let us now see what we can tell about the extra energy term for $\mu_{12} \neq 0$ (and, naturally, with $\kappa \neq 0$). We can start using (52), and then we can substitute (51):

$$\frac{\kappa}{2\varrho}\eta^2 = \frac{\kappa}{2\varrho}\left[-\big(\mu_{21}L + \mu_{22}\kappa\dot{\eta}\big)\right]^2 = \frac{\kappa}{2\varrho}\left[\mu_{21}L + \mu_{22}\kappa\frac{\hat{\sigma} - \mu_{11}L}{\mu_{12}\kappa}\right]^2 =$$

$$= \frac{\kappa}{2\varrho\mu_{12}^2\kappa^2}\left[\mu_{21}\mu_{12}\kappa L + \mu_{22}\kappa\hat{\sigma} - \mu_{11}\mu_{22}\kappa L\right]^2 = \frac{1}{2\varrho\mu_{12}^2\kappa}\left[\tau\hat{\sigma} - \hat{\hat{E}}L\right]^2 =$$

$$= \frac{\chi}{2\varrho}\Lambda^2\,, \qquad \text{where} \quad \chi = \frac{1}{\kappa\mu_{12}^2}\,, \quad \Lambda = \tau\hat{\sigma} - \hat{\hat{E}}L\,. \tag{61}$$

Hence, via rescaling of the internal variable (which is a legitimate step since κ was a free parameter and there was no convention fixing on η, either), it can be understood as a combination of the kinematically well-interpretable L, the mechanically well-interpretable $\hat{\sigma}$, and the (experimentally fittable) coefficients τ, $\hat{\hat{E}}$ of the Kluitenberg–Verhás model. Let us identify this rescaling explicitly: expressing $\dot{\eta}$ from (51), and substituting it into (52),

$$\eta = \frac{-1}{\kappa\mu_{12}}\Lambda\,. \tag{62}$$

Let us investigate the thermodynamical restrictions on χ: in terms of the *index of inertia*

$$\hat{\mathring{I}} := \hat{\mathring{E}} - \tau\hat{I} = \kappa \det \mu - \kappa\mu_{22}\mu_{11} = -\kappa\mu_{12}\mu_{21}, \tag{63}$$

we can deduce

$$0 \le \kappa \det \mu^{\mathsf{S}} = \kappa\mu_{11}\mu_{22} - \kappa\left(\frac{\mu_{12}+\mu_{21}}{2}\right)^2 = \tau\hat{I} - \kappa\frac{\mu_{12}\mu_{21}}{2} - \frac{\kappa}{4}\left(\mu_{12}^2+\mu_{21}^2\right), \tag{64}$$

$$\frac{\kappa}{4}\left(\mu_{12}^2+\mu_{21}^2\right) \le \tau\hat{I} + \frac{\hat{\mathring{I}}}{2}, \qquad \frac{\kappa}{4}\left(\mu_{12}^2 + \frac{\hat{\mathring{I}}^2}{\kappa^2\mu_{12}^2}\right) \le \tau\hat{I} + \frac{\hat{\mathring{I}}}{2},$$
$$\kappa^2\mu_{12}^4 + \hat{\mathring{I}}^2 \le 2\left(2\tau\hat{I} + \hat{\mathring{I}}\right)\kappa\mu_{12}^2, \tag{65}$$

$$\left(\kappa\mu_{12}^2\right)^2 - 2\left(2\tau\hat{I} + \hat{\mathring{I}}\right)\left(\kappa\mu_{12}^2\right) + \hat{\mathring{I}} \le 0. \tag{66}$$

This is a second-order algebraic inequality, the solution of which is

$$\left(2\tau\hat{I} + \hat{\mathring{I}}\right) - \sqrt{\left(2\tau\hat{I} + \hat{\mathring{I}}\right)^2 - \hat{\mathring{I}}^2} \le \kappa\mu_{12}^2 \le \left(2\tau\hat{I} + \hat{\mathring{I}}\right) + \sqrt{\left(2\tau\hat{I} + \hat{\mathring{I}}\right)^2 - \hat{\mathring{I}}^2}. \tag{67}$$

This, replacing $\hat{\mathring{I}}$ with $\hat{\mathring{E}} - \tau\hat{I}$, can be rewritten after simple algebraic steps into the following informative form:

$$\left(\sqrt{\tau\hat{I}} - \sqrt{\hat{\mathring{E}}}\right)^2 \le \kappa\mu_{12}^2 \le \left(\sqrt{\tau\hat{I}} + \sqrt{\hat{\mathring{E}}}\right)^2. \tag{68}$$

These conditions become irrelevant if $\kappa = 0$ or $\mu_{12} = 0$. If neither of them is zero, then

$$\frac{1}{\left(\sqrt{\tau\hat{I}} + \sqrt{\hat{\mathring{E}}}\right)^2} \le \chi \le \frac{1}{\left(\sqrt{\tau\hat{I}} - \sqrt{\hat{\mathring{E}}}\right)^2} \tag{69}$$

emerges from the second law-imposed inequalities. [τ, $\hat{I}$, $\hat{\mathring{E}}$ are non-negative so the lower bound here is always well-defined. In parallel, for $\hat{\mathring{E}} = \tau\hat{I}$ (*i.e.,* for $\hat{\mathring{I}} = 0$), the upper bound is ∞, with $<$ instead of $\le$ before it.]

If at least one of τ, $\hat{I}$, or $\hat{\mathring{E}}$ is zero then the lower and upper bounds are equal, consequently, χ is uniquely determined. It is easy to check that then we happen to reproduce the extra energy term obtained directly in Sects. 5–7. On the other side, in the case of a full Kluitenberg–Verhás model, χ moves freely within an interval. Its value can be experimentally fitted only from caloric information – most easily from measuring temperature. Namely, the model predicts the time derivative of temperature as follows: similarly as above, we use (50), replacing η with its form (62), and substituting $\dot{\eta}$ expressed from (61), finding

$$\varrho\frac{\mathrm{d}e_{\mathrm{th}}}{\mathrm{d}T}\dot{T} = \varrho\dot{e}_{\mathrm{th}} = \hat{\sigma}L - \kappa\eta\dot{\eta} = \hat{\sigma}L + \chi\left(\hat{\sigma} - \hat{I}L\right)\Lambda, \tag{70}$$

and this contains χ and kinematically and mechanically accessible quantities, consequently, χ can be determined from experimental data.

9. Comparison of the presented rheological models

Before proceeding, it is instructive to visualize the relationships among the rheological models introduced so far, and to compare the typical behaviours of these models. Figure 2 displays the relationships.

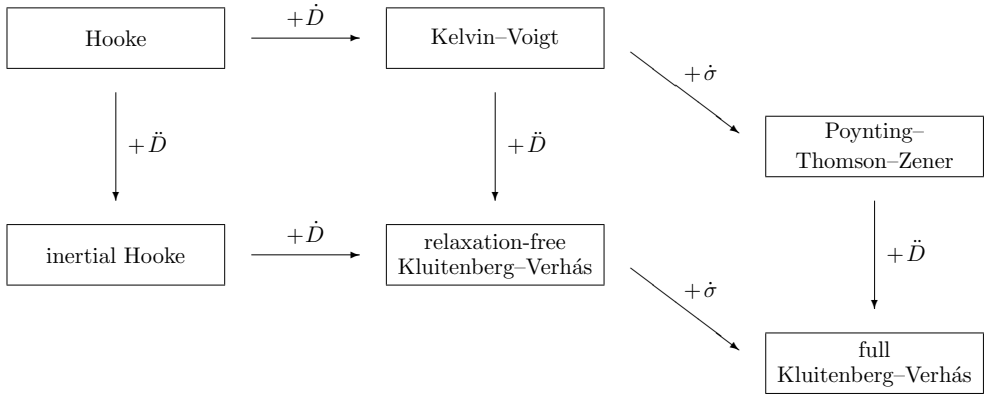

Figure 2. From Hooke to Kluitenberg–Verhás: relationships among the presented rheological models.

Next, Figure 3 shows the different time dependencies $D(t)$ in different rheological models for the same prescribed stress history. Some remarkable observations are as follows.

- As expected, the Hooke model ($\sigma = ED$) mimics what happens to stress.
- The inertial Hooke model $\left(\sigma = ED + \hat{\hat{E}}\ddot{D}\right)$ oscillation around the Hooke prediction.
- The Poynting–Thomson–Zener model $\left(\sigma + \tau\dot{\sigma} = ED + \hat{E}\dot{D}\right)$ also presents a corner when stress has a corner, which can be illustrated as follows: for fast changes, among the σ terms only the highest time derivative term is relevant, and among the D terms only the highest time derivative term is relevant, hence, $\tau\dot{\sigma} \approx \hat{E}\dot{D}$, and integrating this along a small enough time interval gives $\tau\Delta\sigma \approx \hat{E}\Delta D$, $\Delta\sigma/\Delta D \approx \hat{E}/\tau$ (dynamic Young's modulus), meaning a Hooke-like fast response. Finally, for corners, this reasoning can be generalized from functions to distributions. (Note that a sharp corner can be conceived as a limit of a sequence of smooth turns, sharper-and-sharper ones.)

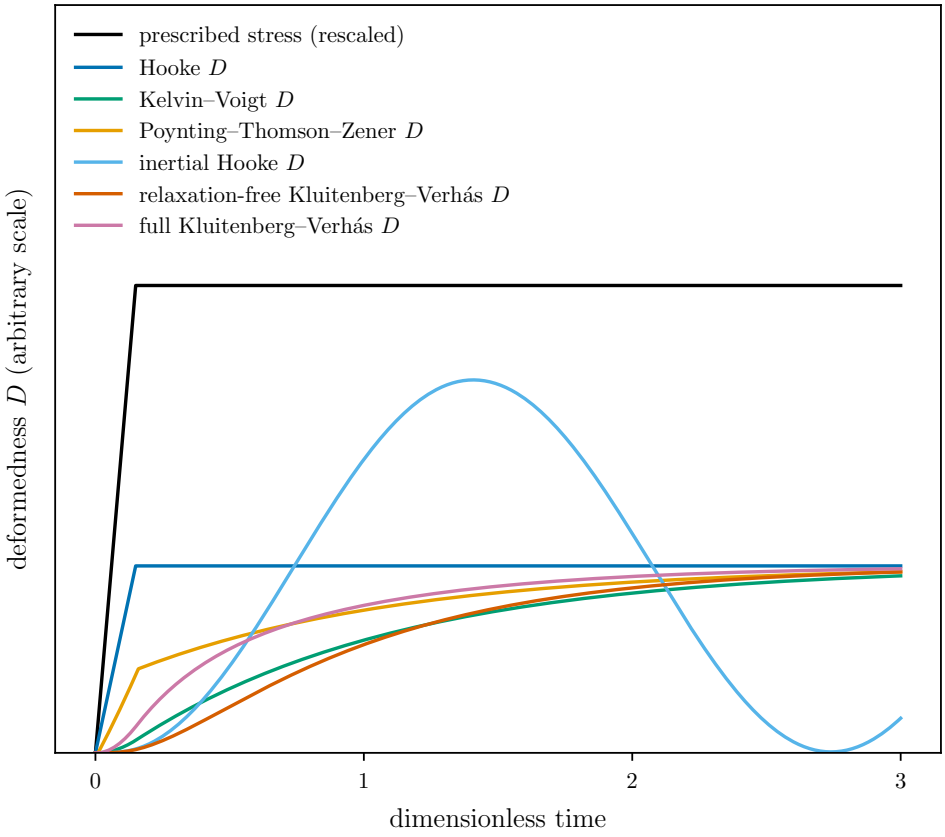

Figure 3. Behaviour of the Kluitenberg–Verhás model and its special subfamilies for $\tau = 0.4t_{\text{unit}}$ and $\hat{\hat{E}} = 0.8t_{\text{unit}}^2 E$, using the time scale $\hat{E}/E$ as the time unit t_{unit} (the vertical scale being arbitrary since all these models are linear), when stress is increased linearly in time until instant $0.15t_{\text{unit}}$ and then it is kept constant.

- The Poynting–Thomson–Zener model $\left(\sigma + \tau\dot{\sigma} = ED + \hat{E}\dot{D}\right)$ also presents a corner when stress has a corner, which can be illustrated as follows: for fast changes, among the σ terms only the highest time derivative term is relevant, and among the D terms only the highest time derivative term is relevant, hence, $\tau\dot{\sigma} \approx \hat{E}\dot{D}$, and integrating this along a small enough time interval gives $\tau\Delta\sigma \approx \hat{E}\Delta D$, $\Delta\sigma/\Delta D \approx \hat{E}/\tau$ (dynamic Young's modulus), meaning a Hooke-like fast response. Finally, for corners, this reasoning can be generalized from functions to distributions. (Note that

a sharp corner can be conceived as a limit of a sequence of smooth turns, sharper-and-sharper ones.)

- The rest of the considered rheological models [Kelvin–Voigt $\left(\sigma = ED + \hat{E}\dot{D}\right)$, relaxation-free Kluitenberg–Verhás $\left(\sigma = ED + \hat{E}\dot{D} + \hat{\hat{E}}\ddot{D}\right)$, full Kluitenberg–Verhás $\left(\sigma + \tau\dot{\sigma} = ED + \hat{E}\dot{D} + \hat{\hat{E}}\ddot{D}\right)$] have a higher order time derivative of D than that of σ so these further models react more smoothly to an abrupt stress change.
- Except for Hooke and inertial Hooke, all models tend irreversibly to the stationary Hooke prediction.

10. Thermal expansion: the initial model

In the presence of thermal expansion, L is no longer equal to $\dot{D}$: the kinematic changes are not only elastic deviation type but thermal expansion type as well. Closer (and tensorial) formulation is provided in [18, 22–27], here, only the small-deformation (and first only "one-dimensional" – one kinematic degree of freedom) formula

$$L = \dot{D} + \alpha\dot{T} \tag{71}$$

is needed, in which the linear thermal expansion coefficient α will be considered constant, for better readability and ease in application. The works [18, 22–27] also provide the consistent thermomechanical background of elastic plus thermal-expansion phenomena. This Hooke plus thermal-expansion model will be the initial model – the starting point – for deriving the Kluitenberg–Verhás plus thermal expansion model. Stress remains unmodified as a function of D,

$$\sigma = ED \tag{72}$$

(as the cited works show, if $D_{\text{initial}} = 0$ then replacing D with ε yields the classic Duhamel–Neumann formula). On the other side, e and s become generalized:

$$e(T, D) = e_{\text{th}}(T) + \frac{\alpha E}{\varrho} TD + \frac{E}{2\varrho} D^2 , \tag{73}$$

$$s(T, D) = s_{\text{th}}(T) + \frac{\alpha E}{\varrho} D . \tag{74}$$

This initial model is reversible and nondissipative:

$$\begin{aligned} T\pi_S &= \varrho T\dot{s} = \varrho T \frac{\mathrm{d}s_{\text{th}}}{\mathrm{d}T}\dot{T} + \varrho T \frac{\alpha E}{\varrho}\dot{D} = \varrho \frac{\mathrm{d}e_{\text{th}}}{\mathrm{d}T}\dot{T} + \varrho T \frac{\alpha E}{\varrho}\dot{D} = \\ &= \varrho\dot{e}_{\text{th}} + T \cdot \alpha E\dot{D} = \varrho\left(e - \frac{\alpha E}{\varrho} TD - \frac{E}{2\varrho} D^2\right)^{\cdot} + \alpha ET\dot{D} = \\ &= \sigma L - \alpha E\left(\dot{T}D + T\dot{D}\right) - ED\dot{D} + \alpha ET\dot{D} = \\ &= ED\left(\dot{D} + \alpha\dot{T}\right) - \alpha E\dot{T}D - \alpha ET\dot{D} - ED\dot{D} + \alpha ET\dot{D} = 0 . \end{aligned} \tag{75}$$

As a consequence, temperature is no longer time-independent:

$$0 = T\pi_S = \cdots = \varrho \frac{\mathrm{d}e_{\mathrm{th}}}{\mathrm{d}T}\dot{T} + \varrho T \frac{\alpha E}{\varrho}\dot{D} \qquad \Longrightarrow \qquad \frac{\mathrm{d}e_{\mathrm{th}}}{\mathrm{d}T}\dot{T} = -T\frac{\alpha E}{\varrho}\dot{D}. \tag{76}$$

11. Extension of the Kluitenberg–Verhás model to include thermal expansion

We assume again an extra stress contribution

$$\hat{\sigma} = \sigma - ED\,, \tag{77}$$

and we shift e by a term as before:

$$e(T, D, \eta) = e_{\mathrm{th}}(T) + \frac{\alpha E}{\varrho}TD + \frac{E}{2\varrho}D^2 + \frac{\kappa}{2\varrho}\eta^2\,, \tag{78}$$

while s is kept untouched. (75) becomes extended due to the mechanical power contribution $\hat{\sigma}L$ and via the time derivative of the extra (rheological) specific energy term:

$$T\pi_S = \cdots = \hat{\sigma}L - \kappa\eta\dot{\eta}\,. \tag{79}$$

Starting from here, formulae (51)–(55) and (58)–(69) all remain valid. (Not by coincidence: as a precaution, they have been formulated in such a way that they are not influenced by the appearance of thermal expansion.) The relationship $L = \dot{D}$ was used in (56)–(57), their generalization for thermal expansion is

$$\sigma - ED + \tau\left(\dot{\sigma} - E\dot{D}\right) = \hat{I}L + \hat{\hat{E}}\dot{L}\,, \tag{80}$$

$$\sigma + \tau\dot{\sigma} = ED + \tau E\dot{D} + \hat{I}\left(\dot{D} + \alpha\dot{T}\right) + \hat{\hat{E}}\left(\ddot{D} + \alpha\ddot{T}\right)\,, \tag{81}$$

$$\sigma + \tau\dot{\sigma} = ED + \hat{E}\dot{D} + \hat{\hat{E}}\ddot{D} + \hat{I}\alpha\dot{T} + \hat{\hat{E}}\alpha\ddot{T}\,. \tag{82}$$

In addition, for expressing the time derivative of temperature, (70) is to be generalized: (76) remains valid to the extent that

$$T\pi_S = \cdots = \varrho \frac{\mathrm{d}e_{\mathrm{th}}}{\mathrm{d}T}\dot{T} + \varrho T \frac{\alpha E}{\varrho}\dot{D}\,. \tag{83}$$

In parallel, (79) is also rewritable as in (70):

$$T\pi_S = \hat{\sigma}L - \kappa\eta\dot{\eta} = \hat{\sigma}L + \chi\left(\hat{\sigma} - \hat{I}L\right)\Lambda\,, \tag{84}$$

therefore,

$$\varrho \frac{\mathrm{d}e_{\mathrm{th}}}{\mathrm{d}T}\dot{T} = -\varrho T \frac{\alpha E}{\varrho}\dot{D} + \hat{\sigma}L + \chi\left(\hat{\sigma} - \hat{I}L\right)\Lambda\,. \tag{85}$$

12. The three-dimensional tensorial variant

In the three-dimensional (3D) treatment, we restrict the discussion to isotropic materials. Also, we remain in the small-deformation regime.[8] $\boldsymbol{\sigma}$ and $\mathbf{D}$ are symmetric tensors so the internal variable $\boldsymbol{\eta}$ with a mechanical role is also chosen to be a symmetric tensor. Knowledge of the decomposition of symmetric tensors to deviatoric ($^{\mathrm{dev}}$) and spherical ($^{\mathrm{sph}}$) parts and the corresponding basic properties (*e.g.,* that the trace of the product of a deviatoric tensor and a spherical tensor is zero) will be assumed (see, *e.g.,* [18], and [8] is also useful for the aspects in the present context). Because of this decoupling of deviatoric and symmeric parts, the deviatoric part can be viewed as a model with one kinematic degree of freedom ("1D") (a)nd free of thermal expansion because thermal expansion is also isotropic, while the spherical part is also effectively 1D (but contains thermal expansion).[9]

The 3D Kluitenberg–Verhás model extended to include thermal expansion is as follows. Kinematically, the relationship among the kinematically involved quantities is

$$\mathbf{L}^{\mathsf{S}} = \dot{\mathbf{D}} + \alpha \dot{T} \mathbf{1} \tag{86}$$

[18, 22–27]. The deviation $\hat{\boldsymbol{\sigma}}$ of stress from the Hooke–Duhamel–Neumann elastic one is

$$\hat{\boldsymbol{\sigma}}^{\mathrm{dev}} = \boldsymbol{\sigma}^{\mathrm{dev}} - E^{\mathrm{dev}} \mathbf{D}^{\mathrm{dev}}, \qquad \hat{\boldsymbol{\sigma}}^{\mathrm{sph}} = \boldsymbol{\sigma}^{\mathrm{sph}} - E^{\mathrm{sph}} \mathbf{D}^{\mathrm{sph}}. \tag{87}$$

Specific internal energy is

$$e(T, \mathbf{D}, \boldsymbol{\eta}) = e_{\mathrm{th}}(T) + \frac{\alpha E^{\mathrm{sph}}}{\varrho} T \operatorname{tr} \mathbf{D} + \frac{E^{\mathrm{dev}}}{2\varrho} \operatorname{tr}\left(\mathbf{D}^{\mathrm{dev}} \mathbf{D}^{\mathrm{dev}}\right) + \frac{E^{\mathrm{sph}}}{2\varrho} \operatorname{tr}\left(\mathbf{D}^{\mathrm{sph}} \mathbf{D}^{\mathrm{sph}}\right) + \\ + \frac{\kappa^{\mathrm{dev}}}{2\varrho} \operatorname{tr}\left(\boldsymbol{\eta}^{\mathrm{dev}} \boldsymbol{\eta}^{\mathrm{dev}}\right) + \frac{\kappa^{\mathrm{sph}}}{2\varrho} \operatorname{tr}\left(\boldsymbol{\eta}^{\mathrm{sph}} \boldsymbol{\eta}^{\mathrm{sph}}\right), \tag{88}$$

and specific entropy is

$$s(T, \mathbf{D}) = s_{\mathrm{th}}(T) + \frac{\alpha E^{\mathrm{sph}}}{\varrho} \operatorname{tr} \mathbf{D}, \tag{89}$$

where (12) is still valid. Analogously to (75),

$$T \pi_S = \dots = \tag{90}$$
$$= \operatorname{tr}\left(\hat{\boldsymbol{\sigma}}^{\mathrm{dev}} \mathbf{L}^{\mathsf{S}^{\mathrm{dev}}}\right) - \kappa^{\mathrm{dev}} \operatorname{tr}\left(\boldsymbol{\eta}^{\mathrm{dev}} \dot{\boldsymbol{\eta}}^{\mathrm{dev}}\right) + \operatorname{tr}\left(\hat{\boldsymbol{\sigma}}^{\mathrm{sph}} \mathbf{L}^{\mathsf{S}^{\mathrm{sph}}}\right) - \kappa^{\mathrm{sph}} \operatorname{tr}\left(\boldsymbol{\eta}^{\mathrm{sph}} \dot{\boldsymbol{\eta}}^{\mathrm{sph}}\right),$$

[8] This enables us to have a linear and mathematically easily treatable framework, which is nevertheless suitable for a broad range of applications. Extension to arbitrary deformations is already a work in progress.

[9] Let us emphasize here that the forthcoming decoupling of the *model* into deviatoric and spherical submodels [(91)–(92)] is a consequence of isotropy, and does not hold for anisotropic materials in general.

the deviatoric and spherical parts are Onsagerically decomposed (due to the isotropy of the material), and $T\pi_S \geq 0$ is ensured by

$$\hat{\boldsymbol{\sigma}}^{\mathrm{dev}} = \mu_{11}^{\mathrm{dev}} \mathbf{L}^{\mathsf{S}^{\mathrm{dev}}} + \mu_{12}^{\mathrm{dev}} \kappa^{\mathrm{dev}} \dot{\boldsymbol{\eta}}^{\mathrm{dev}}, \qquad \hat{\boldsymbol{\sigma}}^{\mathrm{sph}} = \mu_{11}^{\mathrm{sph}} \mathbf{L}^{\mathsf{S}^{\mathrm{sph}}} + \mu_{12}^{\mathrm{sph}} \kappa^{\mathrm{sph}} \dot{\boldsymbol{\eta}}^{\mathrm{sph}}, \tag{91}$$

$$-\boldsymbol{\eta}^{\mathrm{dev}} = \mu_{21}^{\mathrm{dev}} \mathbf{L}^{\mathsf{S}^{\mathrm{dev}}} + \mu_{22}^{\mathrm{dev}} \kappa^{\mathrm{dev}} \dot{\boldsymbol{\eta}}^{\mathrm{dev}}, \qquad -\boldsymbol{\eta}^{\mathrm{sph}} = \mu_{21}^{\mathrm{sph}} \mathbf{L}^{\mathsf{S}^{\mathrm{sph}}} + \mu_{22}^{\mathrm{sph}} \kappa^{\mathrm{sph}} \dot{\boldsymbol{\eta}}^{\mathrm{sph}}, \tag{92}$$

where the coefficients μ_{ij}^{dev}, μ_{ij}^{sph} are constants and fulfil the inequalities

$$\mu_{11}^{\mathrm{dev}} \geq 0, \qquad \mu_{22}^{\mathrm{dev}} \geq 0, \qquad \mu_{11}^{\mathrm{dev}} \mu_{22}^{\mathrm{dev}} - \left(\frac{\mu_{12}^{\mathrm{dev}} + \mu_{21}^{\mathrm{dev}}}{2} \right)^2 \geq 0, \tag{93}$$

$$\mu_{11}^{\mathrm{sph}} \geq 0, \qquad \mu_{22}^{\mathrm{sph}} \geq 0, \qquad \mu_{11}^{\mathrm{sph}} \mu_{22}^{\mathrm{sph}} - \left(\frac{\mu_{12}^{\mathrm{sph}} + \mu_{21}^{\mathrm{sph}}}{2} \right)^2 \geq 0. \tag{94}$$

From these Onsagerian coefficients, we define the derived coefficients

$$\tau^{\mathrm{dev}} := \kappa^{\mathrm{dev}} \mu_{22}^{\mathrm{dev}} \geq 0, \quad \hat{I}^{\mathrm{dev}} := \mu_{11}^{\mathrm{dev}} \geq 0, \quad \hat{E}^{\mathrm{dev}} := \hat{I}^{\mathrm{dev}} + \tau^{\mathrm{dev}} E^{\mathrm{dev}} \geq \tau^{\mathrm{dev}} E^{\mathrm{dev}}, \tag{95}$$

$$\tau^{\mathrm{sph}} := \kappa^{\mathrm{sph}} \mu_{22}^{\mathrm{sph}} \geq 0, \quad \hat{I}^{\mathrm{sph}} := \mu_{11}^{\mathrm{sph}} \geq 0, \quad \hat{E}^{\mathrm{sph}} := \hat{I}^{\mathrm{sph}} + \tau^{\mathrm{sph}} E^{\mathrm{sph}} \geq \tau^{\mathrm{sph}} E^{\mathrm{sph}}, \tag{96}$$

$$\hat{\hat{E}}^{\mathrm{dev}} := \kappa^{\mathrm{dev}} \det \mu^{\mathrm{dev}} \geq 0, \qquad \hat{\hat{I}}^{\mathrm{dev}} := \hat{\hat{E}}^{\mathrm{dev}} - \tau^{\mathrm{dev}} \hat{I}^{\mathrm{dev}}, \tag{97}$$

$$\hat{\hat{E}}^{\mathrm{sph}} := \kappa^{\mathrm{sph}} \det \mu^{\mathrm{sph}} \geq 0, \qquad \hat{\hat{I}}^{\mathrm{sph}} := \hat{\hat{E}}^{\mathrm{sph}} - \tau^{\mathrm{sph}} \hat{I}^{\mathrm{sph}}. \tag{98}$$

These coefficients appear when we remove the internal variable, obtaining

$$\boldsymbol{\sigma}^{\mathrm{dev}} + \tau^{\mathrm{dev}} \dot{\boldsymbol{\sigma}}^{\mathrm{dev}} = E^{\mathrm{dev}} \mathbf{D}^{\mathrm{dev}} + \hat{E}^{\mathrm{dev}} \dot{\mathbf{D}}^{\mathrm{dev}} + \hat{\hat{E}}^{\mathrm{dev}} \ddot{\mathbf{D}}^{\mathrm{dev}}, \tag{99}$$

$$\boldsymbol{\sigma}^{\mathrm{sph}} + \tau^{\mathrm{sph}} \dot{\boldsymbol{\sigma}}^{\mathrm{sph}} = E^{\mathrm{sph}} \mathbf{D}^{\mathrm{sph}} + \hat{E}^{\mathrm{sph}} \dot{\mathbf{D}}^{\mathrm{sph}} + \hat{\hat{E}}^{\mathrm{sph}} \ddot{\mathbf{D}}^{\mathrm{sph}} + \hat{I}^{\mathrm{sph}} \alpha \dot{T} \mathbf{1} + \hat{\hat{E}}^{\mathrm{sph}} \alpha \ddot{T} \mathbf{1}. \tag{100}$$

In terms of the combinations

$$\boldsymbol{\Lambda}^{\mathrm{dev}} = \tau^{\mathrm{dev}} \hat{\boldsymbol{\sigma}}^{\mathrm{dev}} - \hat{\hat{E}}^{\mathrm{dev}} \mathbf{L}^{\mathsf{S}^{\mathrm{dev}}}, \qquad \boldsymbol{\Lambda}^{\mathrm{sph}} = \tau^{\mathrm{sph}} \hat{\boldsymbol{\sigma}}^{\mathrm{sph}} - \hat{\hat{E}}^{\mathrm{sph}} \mathbf{L}^{\mathsf{S}^{\mathrm{sph}}}, \tag{101}$$

the extra/rheological energy terms are nonzero if at least one of τ^{dev}, $\hat{I}^{\mathrm{dev}}$, $\hat{\hat{E}}^{\mathrm{dev}}$ is nonzero and if at least one of τ^{sph}, $\hat{I}^{\mathrm{sph}}$, $\hat{\hat{E}}^{\mathrm{sph}}$ is nonzero, respectively, and then these extra terms are

$$\frac{\chi^{\mathrm{dev}}}{2\varrho} \operatorname{tr}\left(\boldsymbol{\Lambda}^{\mathrm{dev}} \boldsymbol{\Lambda}^{\mathrm{dev}} \right) \qquad \text{resp.} \qquad \frac{\chi^{\mathrm{sph}}}{2\varrho} \operatorname{tr}\left(\boldsymbol{\Lambda}^{\mathrm{sph}} \boldsymbol{\Lambda}^{\mathrm{sph}} \right), \tag{102}$$

where

$$\frac{1}{\left(\sqrt{\tau^{\mathrm{dev}}\hat{I}^{\mathrm{dev}}}+\sqrt{\hat{\hat{E}}^{\mathrm{dev}}}\right)^2}\leq\chi^{\mathrm{dev}}\leq\frac{1}{\left(\sqrt{\tau^{\mathrm{dev}}\hat{I}^{\mathrm{dev}}}-\sqrt{\hat{\hat{E}}^{\mathrm{dev}}}\right)^2}\,, \tag{103}$$

$$\frac{1}{\left(\sqrt{\tau^{\mathrm{sph}}\hat{I}^{\mathrm{sph}}}+\sqrt{\hat{\hat{E}}^{\mathrm{sph}}}\right)^2}\leq\chi^{\mathrm{sph}}\leq\frac{1}{\left(\sqrt{\tau^{\mathrm{sph}}\hat{I}^{\mathrm{sph}}}-\sqrt{\hat{\hat{E}}^{\mathrm{sph}}}\right)^2}\,. \tag{104}$$

The equation expressing the time evolution of temperature is

$$\varrho\frac{\mathrm{d}e_{\mathrm{th}}}{\mathrm{d}T}\dot{T}=-\varrho T\frac{\alpha E^{\mathrm{sph}}}{\varrho}\,\mathrm{tr}\,\dot{\mathbf{D}}+\mathrm{tr}\left(\hat{\boldsymbol{\sigma}}^{\mathrm{dev}}\mathbf{L}^{\mathsf{S}^{\mathrm{dev}}}\right)+\chi^{\mathrm{dev}}\,\mathrm{tr}\left[\left(\hat{\boldsymbol{\sigma}}^{\mathrm{dev}}-\hat{I}^{\mathrm{dev}}\mathbf{L}^{\mathsf{S}^{\mathrm{dev}}}\right)\boldsymbol{\Lambda}^{\mathrm{dev}}\right]+$$
$$+\,\mathrm{tr}\left(\hat{\boldsymbol{\sigma}}^{\mathrm{sph}}\mathbf{L}^{\mathsf{S}^{\mathrm{sph}}}\right)+\chi^{\mathrm{sph}}\,\mathrm{tr}\left[\left(\hat{\boldsymbol{\sigma}}^{\mathrm{sph}}-\hat{I}^{\mathrm{sph}}\mathbf{L}^{\mathsf{S}^{\mathrm{sph}}}\right)\boldsymbol{\Lambda}^{\mathrm{sph}}\right]. \tag{105}$$

13. Heat conduction

For an isotropic material, heat conduction can be incorporated in a straightforward way in the continuum description: Fourier's law

$$\mathbf{j}_E=-\lambda\nabla T \tag{106}$$

is to be added to the set of equations, and the corresponding energy balance (2) is to be considered (from which the time derivative of temperature can be obtained). No complication can arise since Onsagerian coupling is not possible between the tensorial mechanical quantities and the vectorial heat current density [7, 19].

For the special subfamily of Poynting–Thomson–Zener standard rheology coupled to heat conduction via thermal expansion, numerical solutions in one space dimension have been presented in [31]. So far, no corresponding result exists (at least to the author's knowledge) for the Kluitenberg–Verhás generalization.

14. Conclusion

Analyzing the rheology-related additional energy term has provided valuable additional insight into the Kluitenberg–Verhás model and its internal variable, and increased its applicability. The present approach opens the way for generalizing analytical solutions like [6, 32] to include the rheological internal variable as well, and for generalizing numerical solutions of Poynting–Thomson–Zener standard rheology coupled to heat conduction via thermal expansion [31] to the full Kluitenberg–Verhás level.

Generalization of the treatment presented here to *fluids* with any thermodynamically allowed nonlinear constitutive characteristics appears feasible, and is expected to yield a practical non-Newtonian model family {a Jeffreys model for the rheological part of the stress (or pressure) tensor [7]}. In addition, this generalization could be the first step towards the corresponding model family for *solids* with *arbitrary* thermodynamically allowed nonlinear consitutive characteristics *without* the small-deformation

approximation. Hopefully, together with the spacetime-compatible finite-deformation kinematics of solids [22–27], this amalgamation can be done in the near future.

Appendix A. Kluitenberg–Verhás model coefficients fitted on experimental data for some plastic and rock materials

coefficient	value
$\tau^{\mathrm{dev}}/\mathrm{s}$	0.3600
$E^{\mathrm{dev}}/\mathrm{GPa}$	0.8612
$\hat{E}^{\mathrm{dev}}/(\mathrm{GPa}\cdot\mathrm{s})$	0.4724
$\hat{\hat{E}}^{\mathrm{dev}}/\left(\mathrm{GPa}\cdot\mathrm{s}^2\right)$	0.0029
$\tau^{\mathrm{sph}}/\mathrm{s}$	0.2329
$E^{\mathrm{sph}}/\mathrm{GPa}$	4.5708
$\hat{E}^{\mathrm{sph}}/(\mathrm{GPa}\cdot\mathrm{s})$	1.8566
$\hat{\hat{E}}^{\mathrm{sph}}/\left(\mathrm{GPa}\cdot\mathrm{s}^2\right)$	0.0013

Table 1. Fitted rheological coefficients for experimental data obtained on a polyamide-6 sample. Results taken from [5].

coefficient	Granite	Marble	Sandstone
$\tau^{\mathrm{dev}}/\mathrm{h}$	13.15	13.24	16.00
$E^{\mathrm{dev}}/\mathrm{MPa}$	0.82	0.61	0.23
$\hat{E}^{\mathrm{dev}}/(\mathrm{MPa}\cdot\mathrm{h})$	16.46	13.82	6.78
$\hat{\hat{E}}^{\mathrm{dev}}/\left(\mathrm{MPa}\cdot\mathrm{h}^2\right)$	6.38	3.42	10.96
$\tau^{\mathrm{sph}}/\mathrm{h}$	13.97	6.42	2.07
$E^{\mathrm{sph}}/\mathrm{MPa}$	1.65	2.35	0.46
$\hat{E}^{\mathrm{sph}}/(\mathrm{MPa}\cdot\mathrm{h})$	28.44	18.63	5.58
$\hat{\hat{E}}^{\mathrm{sph}}/\left(\mathrm{MPa}\cdot\mathrm{h}^2\right)$	7.66	3.32	2.73

Table 2. Determined rheological coefficients from experimental data obtained on three different types of rock, in 48-hour measurements. Results derived from [4], using the fact that their interpretation in terms of the rheological circuit $\left(E_1 \,||\, \hat{E}_1\right) \sim \left(E_2 \,||\, \hat{E}_2\right)$ ($^{\mathrm{dev}}$ or $^{\mathrm{sph}}$, respectively; $||$ denoting parallel connection and $\sim$ standing for serial connection) is equivalent to $\sigma + \tau\dot{\sigma} = ED + \hat{E}\dot{D} + \hat{\hat{E}}\ddot{D}$ with $\tau = \frac{\hat{E}_1+\hat{E}_2}{E_1+E_2}$, $E = \frac{E_1E_2}{E_1+E_2}$, $\hat{E} = \frac{E_1\hat{E}_2+E_2\hat{E}_1}{E_1+E_2}$, $\hat{\hat{E}} = \frac{\hat{E}_1\hat{E}_2}{E_1+E_2}$ [as is straightforward to find; see, *e.g.,* [11], page 103, Eq. (85)].

In each case (Table 1, Table 2), we can find that $\hat{I} > 0$, fulfilling the second law of thermodynamics. In addition, the $\hat{\hat{I}}$ values turn out to be negative (overdamped case).

For a given material type, the values of these coefficients – and especially the rheological time scales identified from them – provide insight into when the various beyond-Hooke terms in the Kluitenberg–Verhás model play a remarkable role or when their contribution can be neglected. In view of the fact that the rheological time scales can be seconds (see Table 1), hours (as in Table 2), or years [33], it is a good strategy to always be prepared for rheological effects.

Acknowledgement. The author is grateful to Csaba Asszonyi, Gyula Béda, Tamás Matolcsi, Mátyás Szücs, József Verhás, and Péter Ván for related valuable discussions.
The birth of the presented approach was supported by the grants of the Ministry for Innovation and Technology projects NKFIH STARTING 149487 and NKFIH 2018-1.1.2-KFI-2018-00207.

References

[1] Koji Matsuki and K. Takeuchi. "Three-dimensional in situ stress determination by anelastic strain recovery of a rock core." *International Journal of Rock Mechanics and Mining Sciences & Geomechanics Abstracts,* **30**(7), (1993), pp. 1019–1022. DOI: 10.1016/0148-9062(93)90064-K.

[2] Koji Matsuki. "Anelastic strain recovery compliance of rocks and its application to in situ stress measurement." *International Journal of Rock Mechanics and Mining Sciences,* **45**(6), (2008), pp. 952–956. DOI: 10.1016/j.ijrmms.2007.10.005.

[3] W. Lin, Y. Kuwahara, T. Satoh, N. Shigematsu, Y. Kitagawa, T. Kiguchi, and N. Koizumi. "A case study of 3D stress orientation determination in Shikoku Island and Kii Peninsula, Japan." *Rock Engineering in Difficult Ground Conditions – Soft Rock and Karst.* Proceedings of the Regional Symposium of the International Society for Rock Mechanics (ISRM) (Cavtat, Croatia, Oct. 28–29, 2009). Ed. by Ivan Vrkljan. Boca Raton – London – New York – Leiden: CRC Press; Balkema Book, Taylor & Francis Group, 2010, pp. 277–282. URL: https://onepetro.org/ISRMEUROCK/proceedings-abstract/EUROCK09/EUROCK09/ISRM-EUROCK-2009-042/38509.

[4] Lu Gao, Weiren Lin, Dongsheng Sun, and Hongcai Wang. "Experimental anelastic strain recovery compliance of three typical rocks." *Rock Mechanics and Rock Engineering,* **47**, (2014), pp. 1987–1995. DOI: 10.1007/s00603-013-0526-0.

[5] Csaba Asszonyi, Attila Csatár, and Tamás Fülöp. "Elastic, thermal expansion, plastic and rheological processes – theory and experiment." *Periodica Polytechnica Civil Engineering,* **60**(4), (2016), pp. 591–601. DOI: 10.3311/PPci.8628.

[6] Tamás Fülöp and Mátyás Szücs. "Analytical solutions for rheological processes around bores and tunnels." *Journal of Engineering Mathematics,* **136**(1), (2022), pp. 1–28. DOI: 10.1007/s10665-022-10235-6.

[7] József Verhás. *Thermodynamics and Rheology.* Budapest: Akadémiai Kiadó and Kluwer Academic Publisher, 1997. URL: http://montavid.hu/materials/Verhas_Thermodynamics_and_Rheology_2017-05-17.pdf.

[8] Csaba Asszonyi, Tamás Fülöp, and Peter Ván. "Distinguished rheological models for solids in the framework of a thermodynamical internal variable theory." *Continuum Mechanics and Thermodynamics,* **27**(6), (2015), pp. 971–986. DOI: 10.1007/s00161-014-0392-3.

[9] Tamás Fülöp. "Kluitenberg–Verhás-modell, hőtágulás és reológiai energia [Kluitenberg–Verhás model, thermal expansion, and rheological energy]." *Kőzetmechanika és termodinamika [Rock mechanics and thermodynamics].* Ed. by Donát M. Takács, Péter Ván, and Balázs Vásárhelyi. Mérnökgeológia–Kőzetmechanika Kiskönyvtár [Book Series on Engineering Geology and Rock Mechanics] 26. (In Hungarian). Budapest: Egyesület a Tudomány és Technológia Egységéért, 2023. Chap. 8, pp. 129–140. URL: http://montavid.hu/montavid_pdfs/mernokgeologia-kozetmechanika_kiskonyvtar_26.pdf.

[10] TECHNOORG-LINDA. *Az extrém felbontású holografikus mérőkamerával történő "Improved Anelastic Strain Racovery" (IASR) primerfeszültség-mérési eljárás és szolgáltatás kifejlesztése.* (Hungarian-only page. Last accessed 2025-12-28). 2018. URL: https://www.technoorg.hu/about-us/r-and-d-projects/2018-112-kfi-2018-00207.

[11] Tamás Fülöp. "Reológiai elemkapcsolások [Rheological circuits]." *Izotrop kontinuumok anyagtulajdonságai [Material properties of isotropic continua].* Ed. by Csaba Asszonyi. Mérnökgeológia–Kőzetmechanika Kiskönyvtár [Book Series on Engineering Geology and Rock Mechanics] 6. (In Hungarian.) Budapest: Műegyetemi Kiadó, 2008. Chap. 3, pp. 93–120. URL: http://montavid.hu/montavid_pdfs/mernokgeologia-kozetmechanika_kiskonyvtar_06.pdf.

[12] Vito Volterra. *Leçons sur les Fonctions de Lignes.* Paris: Gauthier-Villars, 1913.

[13] Morton E. Gurtin and Eli Sternberg. "On the linear theory of viscoelasticity." *Archive for Rational Mechanics and Analysis,* **11**, (1962), pp. 291–356.

[14] Richard M. Christensen. *Theory of Viscoelasticity. An introduction.* 2nd ed. New York: Academic Press, 1982.

[15] Jörgen Bergström. *Mechanics of Solid Polymers: Theory and Computational Modeling.* Amsterdam etc.: William Andrew – Elsevier, 2015. DOI: 10.1016/C2013-0-15493-1.

[16] J. C. Simo. "On a Fully Three-Dimensional Finite-Strain Viscoelastic Damage Model: Formulation and Computational Aspects." *Computer Methods in Applied Mechanics and Engineering,* **60**, (1987), pp. 153–173. DOI: 10.1016/0045-7825(87)90107-1.

[17] J. C. Simo and T. J. R. Hughes. *Computational Inelasticity.* New York: Springer-Verlag, 1998.

[18] Tamás Fülöp. *Chapters in thermodynamics.* Lecture notes, Budapest University of Technology and Economics. 2024. URL: https://energia.bme.hu/~fulop/Fulop_Chapters_in_Thermodynamics_2024-09-03.pdf.

[19] Sybren Ruurds de Groot and Peter Mazur. *Non-equilibrium thermodynamics.* Amsterdam: Dover Publications, 1962.

[20] Tamás Matolcsi. *Ordinary thermodynamics. Nonequilibrium homogeneous processes*. Budapest: Akadémiai Kiadó (Publishing House of the Hungarian Academy of Sciences), 2004. URL: http://montavid.hu/materials/Matolcsi_Ordinary_Thermodynamics_2017-04-26.pdf.

[21] Tamás Matolcsi. *Közönséges termodinamika [Ordinary thermodynamics]*. (In Hungarian). Budapest: Scolar, 2012.

[22] Tamás Fülöp and Péter Ván. "Véges rugalmas és képlékeny deformációk leírása [Description of finite elastic and plastic deformations]." *Idő- és térderiváltak anyagtörvényekben [Time and space derivatives in material laws]*. Ed. by Tamás Fülöp. Mérnökgeológia–Kőzetmechanika Kiskönyvtár [Book Series on Engineering Geology and Rock Mechanics] 10. (In Hungarian). Budapest: Műegyetemi Kiadó, 2010. Chap. 6, pp. 99–151. URL: http://montavid.hu/montavid_pdfs/mernokgeologia-kozetmechanika_kiskonyvtar_10.pdf.

[23] Tamás Fülöp. "Thermal expansion, elastic stress and finite deformation kinematics." *Proceedings of the 10th HEEP International Conference, 23–25 May 2011, Balatonfüred, Hungary*. Budapest: Department of Energy Engineering, Budapest University of Technology and Economics, 2011, pp. 227–232. URL: http://energia.bme.hu/~fulop/HEEP2011_Proceedings_Papers/40_Tamas.pdf.

[24] Tamás Fülöp and Péter Ván. "Kinematic quantities of finite elastic and plastic deformation." *Mathematical Methods in the Applied Sciences,* **3**(15), (2012), pp. 1825–1841. DOI: 10.1002/mma.2558.

[25] Tamás Fülöp, Péter Ván, and Attila Csatár. "Elasticity, plasticity, rheology and thermal stress – an irreversible thermodynamical theory." *Proceedings of the 12th Joint European Thermodynamics Conference, JETC 2013, Brescia, Italy, July 1–5, 2013*. Ed. by Mariagrazia Pilotelli and Gian Paolo Beretta. Brescia: Cartolibreria SNOOPY, 2013, pp. 525–530. URL: http://energia.bme.hu/~fulop/Fulop-Van-Csatar_2013-Elasticity__plasticity__rheology_and_thermal_stress_-_an_irreversible_thermodynamical_theory-JETC2013-typos_in_Eqs_12_13_17.pdf.

[26] Tamás Fülöp, Péter Ván, and Attila Csatár. "Thermodynamical description of plastic processes." *Proceedings of the 11th HEEP International Conference, June 3–5, 2013, Balatonfüred, Hungary*. Ed. by Gyula Gróf. Budapest: Department of Energy Engineering, Budapest University of Technology and Economics, 2013, pp. 147–152. URL: http://energia.bme.hu/~fulop/HEEP2013_Proceedings.pdf.

[27] Tamás Fülöp. *Objective thermomechanics*. arXiv:1510.08038. 2015. URL: https://arxiv.org/pdf/1510.08038.

[28] Richard B. Hetnarski and M. Reza Eslami. *Thermal stresses – Advanced theory and applications*. Dordrecht: Springer, 2009. DOI: 10.1007/978-1-4020-9247-3.

[29] Péter Ván, Róbert Kovács, and Tamás Fülöp. "Thermodynamic hierarchies of evolution equations," *Proceedings of the Estonian Academy of Sciences.* **64**(3), (2015), pp. 389–395. DOI: 10.3176/PROC.2015.3S.09.

[30] T. Alfrey. *Mechanical Behavior of High Polymers*. New York: Interscience Publ. Co., 1948.

[31] Donát M. Takács, Áron Pozsár, and Tamás Fülöp. "Thermodynamically extended symplectic numerical simulation of viscoelastic, thermal expansion and heat conduction phenomena in solids." *Continuum Mechanics and Thermodynamics,* **36**, (2024), pp. 525–538. DOI: 10.1007/s00161-024-01280-w.

[32] Tamás Fülöp and Mátyás Szücs. "A solution method for determining rheological time dependence around tunnels." *ISRM International Symposium – EUROCK 2020* (Trondheim, Norway, June 14–19, 2020). Ed. by C.C. Li, H. Odegaard, A.H. Hoie, and J. Macias. Lisbon, Portugal: International Society for Rock Mechanics and Rock Engineering, 2020, ISRM–EUROCK–2020–017. URL: https://onepetro.org/ISRMEUROCK/proceedings-abstract/EUROCK20/All-EUROCK20/ISRM-EUROCK-2020-017/447293.

[33] László Kovács, Eszter Mészáros, Ferenc Deák, Gábor Somodi, Kornél Máté, András Jakab, Balázs Vásárhelyi, János Geiger, Gyula Dankó, Ferenc Korpai, Gyula Mező, Krisztián Darvas, Péter Ván, Tamás Fülöp, and Csaba Asszonyi. *A Geotechnikai Értelmező Jelentés (GÉJ) felülvizsgálata és kiterjesztése [Revision and extension of the Geotechnical Interpretation Report]*. Tech. rep. Report RHK-K-032/12. (In Hungarian.) Pécs – Paks: Kőmérő Kft. stored at the repository RHK Kft. Irattára, 2012.

Notes for Contributors
to the Journal of Computational and Applied Mechanics

Aims and scope. The aim of the journal is to publish research papers on theoretical and applied mechanics. Special emphasis is given to articles on computational mechanics, continuum mechanics (mechanics of solid bodies, fluid mechanics, heat and mass transfer) and dynamics. Review papers on a research field and materials effective for teaching can also be accepted and are published as review papers or classroom notes. Papers devoted to mathematical problems relevant to mechanics will also be considered.
Frequency of the journal. Two issues a year (approximately 80 pages per issue).

Submission of Manuscripts. Submission of a manuscript implies that the paper has not been published, nor is being considered for publication elsewhere. Papers should be written in standard grammatical English. The manuscript is to be submitted in electronic, preferably in pdf, format. The text is to be 130 mm wide and 190 mm long and the main text should be typeset in 10pt CMR fonts. Though the length of a paper is not prescribed, authors are encouraged to write concisely. However, short communications or discussions on papers published in the journal must not be longer than 2 pages. Each manuscript should be provided with an English Abstract of about 50–70 words, reporting concisely on the objective and results of the paper. The Abstract is followed by the Mathematical Subject Classification – in case the author (or authors) give the classification codes – then the keywords (no more than five). References should be grouped at the end of the paper in numerical order of appearance. Author's name(s) and initials, paper titles, journal name, volume, issue, year and page numbers should be given for all journals referenced.
The journal prefers the submission of manuscripts in LaTeX. Authors should select the $\mathcal{AMS}$-LaTeX article class and are not recommended to define their own LaTeX commands. Visit our home page for further details concerning how to edit your paper.
Manuscripts should be sent to either to the Editorial Office of JCAM:

jcam@uni-miskolc.hu

or directly to the editor-in-chief: Balázs Tóth

balazs.toth@uni-miskolc.hu

The eventual supply of an accepted for publication paper in its final camera-ready form will ensure more rapid publication. Format requirements are provided by the home page of the journal from which sample LaTeX files can be downloaded:

http://www.mech.uni-miskolc.hu/jcam/

These sample files can also be obtained directly (via e-mail) from Balázs Tóth.

One issue of the journal will be provided free of charge and mailed to the correspondent author. Since JCAM is an open access journal each paper can be downloaded freely from the homepage of the journal.

The Journal of Computational and Applied Mechanics is abstracted in Zentralblatt für Mathematik and in the Russian Referativnij Zhurnal.

Secretariat of the Vice-Rector for Research and International Relations, University of Miskolc
Responsible for publication: Prof. dr. Zita Horváth, rector
Published by the Miskolc University Press under the leadership of Attila Szendi
Responsible for duplication: Works manager Erzsébet Pásztor
Number of copies printed: 50
Put to the Press on March 20, 2026
Number of permission: TSZK.2026-29.ME.
ISSN 2732–0189 (Online)
ISSN 1586–2070 (Print)

A Short History of the Publications of the University of Miskolc

The University of Miskolc (Hungary) is an important center of research in Central Europe. Its parent university was founded by the Empress Maria Teresia in Selmecbánya (today Banska Štiavnica, Slovakia) in 1735. After the first World War the legal predecessor of the University of Miskolc moved to Sopron (Hungary) where, in 1929, it started the series of university publications with the title *Publications of the Mining and Metallurgical Division of the Hungarian Academy of Mining and Forestry Engineering* (Volumes I.–VI.). From 1934 to 1947 the Institution had the name Faculty of Mining, Metallurgical and Forestry Engineering of the József Nádor University of Technology and Economic Sciences at Sopron. Accordingly, the publications were given the title *Publications of the Mining and Metallurgical Engineering Division* (Volumes VII.–XVI.). For the last volume before 1950 – due to a further change in the name of the Institution – *Technical University, Faculties of Mining, Metallurgical and Forestry Engineering, Publications of the Mining and Metallurgical Divisions* was the title.

For some years after 1950 the Publications were temporarily suspended.

After the foundation of the Mechanical Engineering Faculty in Miskolc in 1949 and the movement of the Sopron Mining and Metallurgical Faculties to Miskolc, the Publications restarted with the general title *Publications of the Technical University of Heavy Industry* in 1955. Four new series – Series A (Mining), Series B (Metallurgy), Series C (Machinery) and Series D (Natural Sciences) – were founded in 1976. These came out both in foreign languages (English, German and Russian) and in Hungarian. In 1990, right after the foundation of some new faculties, the university was renamed to University of Miskolc. At the same time the structure of the Publications was reorganized so that it could follow the faculty structure. Accordingly three new series were established: Series E (Legal Sciences), Series F (Economic Sciences) and Series G (Humanities and Social Sciences). The latest series, i.e., the series H (European Integration Studies) was founded in 2001. The eight series are formed by some periodicals and such publications which come out with various frequencies.

Papers on computational and applied mechanics were published in the

Publications of the University of Miskolc, Series D, Natural Sciences.

This series was given the name Natural Sciences, Mathematics in 1995. The name change reflects the fact that most of the papers published in the journal are of mathematical nature though papers on mechanics also come out.

The series

Publications of the University of Miskolc, Series C, Fundamental Engineering Sciences

founded in 1995 also published papers on mechanical issues. The present journal, which is published with the support of the Faculty of Mechanical Engineering and Informatics as a member of the Series C (Machinery), is the legal successor of the above journal.

Journal of Computational and Applied Mechanics

Volume 20, Number 2 (2025)

Contents

Contributed Papers